Mathematisches Forschungsinstitut Oberwolfach

Report No. 29/2009

DOI: 10.4171/OWR/2009/29

Computational Multiscale Methods

Organised by
Carsten Carstensen, Berlin/Seoul
Björn Engquist, Austin/Stockholm

June 14th – June 20th, 2009

Abstract. Computational Multiscale Methods play an important role in many modern computer simulations in material sciences with different time scales and different scales in space. Besides various computational challenges, the meeting brought together various applications from many disciplines and scientists from various scientific communities.

Mathematics Subject Classification (2000): 65N, 35B, 74Q, 70F, 76A, 76M, 94A, 65R.

Introduction by the Organisers

The computer simulation of problems with various scales is relevant almost everywhere in applications ranging from material design with microstructures in engineering to atomistic phenomena in macroscopic simulations in physics and biology. The Oberwolfach workshop *Computational Multiscale Methods* brought together well-established and younger scientists from various communities to study and discuss an emergence of methods that replace heuristics and empirical observations in coarse scale physics by direct numerical simulations of more accurate models defined on finer scales. This is a timely topic since computers are now powerful enough for these simulations, but it is still far from achievable to just use microscale computations for most macroscale phenomena. The development of mathematical analysis and new numerical algorithms that can couple the different scales are needed to fill in the gap.

Multiple scales in layers-within-layers microstructures in material sciences of solids were an important topic during the meeting. Georg Dolzmann discussed an overall algorithm with numerical relaxation on the microscopic scales and the issue of data representation. The computational approaches to time evolving models

were discussed by Klaus Hackl and Tomas Roubichek with a focus on shape memory alloys and rate-independent processes as they arise naturally e.g. in elastoplasticity. Wolfgang Hackbusch suggested the use of H-matrices in some direct approximation of some projected inverse on the fine-scale to compute efficiently on coarser scales. Ralf Kornhuber proposed a hierarchical domain decomposition algorithm to separate fractures from the porous matrix. Uri Ascher applied fast multiscale algorithms in the denoising of 3D surface meshes with fine scale textures and sharp edges.

The efficient computation in multiscale algorithms leads to new directions in the numerical analysis. Giovanni Samaey illustrated the use of approximate coarse-scale models in equation-free multiscale algorithms. To run large multiscale problems on parallel computers, Alfonso Caiazzo set a framework for distributed multiscale simulations.

A further new aspect is the a posteriori error estimation and the assessment of computed approximations on all scales. Axel Malquist and Serge Prudhomme reported on adaptive multiscale modeling via numerical homogenization and adaptive variational multiscale methods.

The quasicontinuum approximation is an effective way to compute a large number of particles, as Ping Lin pointed out for static and dynamic applications. Frederic Legoll justified a reduced model for an effective computation in material science by asymptotic tools of probability at constant temperature. Mitchell Luskin discussed sharp stability estimates for some popular atomistic-to-continuum coupling methods currently used by scientists and engineers. He proposed that these kind of sharp stability estimates are essential for evaluating the predictive capability of such atomistic-to-continuum coupling methods for atomistic instabilities such as fractures, dislocation movement, or crack tip propagation and discussed several examples. He also discussed the need to distinguish whether the breakdown of an error analysis before atomistic instability is an artifact of the analysis, or whether the particular quasicontinuum method actually predicts an instability incorrectly. Pingbing Ming presented a multigrid method for molecular mechanics based on the Cauchy-Born rule. Besides the huge number of particles, the different time-scales are a numerical challenge as pointed out by Petr Plechac during his presentation of the implicit mass-matrix penalization for the numerical integration and sampling of large particle systems with dynamics on multiple scales. Yi Sun investigated the heterogeneous multiscale method for simulating epitaxial growth and neuronal network dynamics with kinetic Monte-Carlo simulations. Anders Szepessy discussed the accuracy of molecular dynamics and accurate approximations of the time-independent Schrödinger observables named after Born-Oppenheimer, Smoluchowski, Langevin, and Ehrenfest.

Besides mathematicians, some leading engineers on computational micromechanics presented their vision and algorithms. Peter Wriggers exploited the FE^2 method, which employs one macroscopic finite element mesh and, for each material point under consideration in some numerical quadrature, some further

discretisation to model the fine material properties. The computations on the fine scales are very costly and so Jörg Schöder and Daniel Balzani suggested some further approximation of the microscopic material by some substitute computed by some least-square fit under the constraint of conserving several statistical characteristic quanitities. Each justification of this and the balance of various discretisation errors on the different levels of the FE^2 computation were vividly discussed. The efficient multiscale analysis for non-linear structural problems was highlighted by Olivier Allix.

Not only multiscale problems in solids were studied during this week. Weiqing Ren discussed multiscale problems in complex fluid flow simulation. He suggested a special coupling of marco- and micro-models in connection with the evolution of such fluids. The mechanical behaviour of biomembranes in the liquid crystal phase was discussed by Pingwen Zhang. Some hybrid particle-continuum method was introduced by Alexander Donev for the hydrodynamics of polymer chains. Eun-Jae Park studied conservative multiscale methods for Darcy-type equations.

The aforementioned algorithms are essentially based on a separation of scales and there were also visions beyond that during the workshop. Leonid Berlyand explained his transfer-property approach to the homogenization of problems with non-separated scales. Daniel Peterseim responded and presented the first finite element analysis of particle reinforced composites with comparable numerical results.

This workshop on Computational Multiscale Methods clearly demonstrated that the field is very active and currently enjoys great progress with many new important results. The workshop also demonstrated that further development of computational multiscale methods strongly benefits from interaction between mathematical analysts, computational experts, and scientists from the many fields with multiscale systems. Many promising results were presented and it is clear that in the future more challenging multiscale processes can be computed with first principle or microscale accuracy even for system wide or macroscale phenomena.

Workshop: Computational Multiscale Methods

Table of Contents

Abstracts

Fast denoising of 3D surface meshes with fine scale texture and sharp features

Uri Ascher
(joint work with Hui Huang)

Grahics objects are typically represented in 3D by a triangle surface mesh. We discuss techniques for faithfully reconstructing such surface models with different features. Some such objects contain visually meaningful components on different scales or detail, and typically require very fine meshes to represent them well. Others consist of large flat regions, long sharp edges and distinct corners, and the required mesh for adequate representation can often be much coarser. All of these models may be sampled very irregularly, unlike in typical image processing applications.

For models of the first class, we methodically develop a fast multiscale anisotropic Laplacian (MSAL) smoothing algorithm that is capable of retaining fine scale texture as well as mesh irregularities [1].

To reconstruct a piecewise smooth CAD-like model in the second class, we design an efficient hybrid algorithm involving the multiscale algorithm of [1] and based on specific vertex classification, which combines K-means clustering and geometric a priori information. While denoising, our method simultaneously regularizes over featureless regions and preserves edge sharpness [2]. Hence we have a set of algorithms that efficiently handle smoothing and regularization of meshes large and small in a variety of situations.

References

[1] H. Huang and U. Ascher. Fast denoising of surface meshes with intrinsic texture. Inverse Problems, 24 (3):034003, 2008.

[2] H. Huang and U. Ascher. Surface mesh smoothing, regularization and feature detection. SIAM J. Scient. Comput., 31:74?93, 2008.

Statistically Similar RVEs for FE^2-Simulations

Daniel Balzani
(joint work with Jörg Schröder, Dominik Brands)

1. Introduction

A suitable numerical tool for the prediction of the mechanical behavior of micro-heterogeneous materials, as e.g. advanced high strength steels, is the FE^2-method, see e.g. Smit et al. [7], Miehe et al. [4], Schröder [6]. In this context a micromechanical boundary value problem is solved at each macroscopic Gauss point, where the discretization of a representative volume element (RVE) reflecting the real microstructure is taken into account. In order to obtain an efficient simulation tool which leads to reduced computational costs less complex RVEs are required. A method for the determination of substructures that are statistically similar to more complex two-phase microstructures with fixed inclusion morphologies is proposed in Povirk [5]. There, the author optimizes a periodic statistically similar substructure by minimizing a least square function considering the power spectral densities of the real microstructure and the substructure, where only a simple geometry of the inclusions is considered. Motivated by this work we propose a more general method for the generation of statistically similar RVEs (SSRVEs) much smaller than typical RVEs, cf. [1], [3] and where an arbitrary morphology of the inclusion phase can be taken into account.

2. Construction of Statistically Similar RVEs

Here, the SSRVE is obtained by minimizing a least-square functional accounting for the volume fraction and the spectral densities (SD's) of a given random microstructure (target structure) and the SSRVE to be generated. For this purpose we consider the objective function

$$\mathcal{L}(\boldsymbol{\gamma}) := \frac{1}{N_x\, N_y} \sum_{m=1}^{N_x} \sum_{k=1}^{N_y} \left(\mathcal{P}_{SD}^{real}(m,k) - \mathcal{P}_{SD}^{SSRVE}(m,k,\boldsymbol{\gamma})\right)^2 + \left(1 - \frac{\mathcal{P}_V^{SSRVE}(\boldsymbol{\gamma})}{\mathcal{P}_V^{real}}\right)^2$$

which should become minimal. The statistical measures describing the inclusion phase of the given (real) microstructure and the SSRVE are denoted by $(\bullet)^{real}$ and $(\bullet)^{SSRVE}$. The first statistical measure is the discrete spectral density

$$\mathcal{P}_{SD}(m,k) := \frac{|\mathcal{F}(m,k)|^2}{2\pi N_x N_y} \text{ with } \mathcal{F} = \sum_{p=1}^{N_x} \sum_{q=1}^{N_y} \exp\left(\frac{2i\pi mp}{N_x}\right) \exp\left(\frac{2i\pi kq}{N_y}\right) \chi(p,q)\,,$$

wherein the discrete Fourier transform $\mathcal{F}$ is mainly governed by the indicator function χ defined to be equal to one if the position is in the inclusion phase and equal to zero else. In addition to that we consider the volume fraction $\mathcal{P}_V$ of the inclusion phase as an additional penalty term in the objective function. The vector $\boldsymbol{\gamma}$ describes the parameterization of the two-dimensional inclusion phase morphology; here it consists of the coordinates of sampling points of splines which are used

for the parameterization. In order to get reasonable results it may be necessary not to consider the spectral density at a very fine resolution level. Therefore, first the SD is computed at a high resolution, then it is rebinned such that a lower resolution is obtained, then it is normalized and finally a relevant area is extracted by defining a threshold value, for details see [3].
A specific discrete image resolution is obviously the computation base for the spectral density and the volume fraction. Hence, this leads to a non-smooth function and precludes the application of standard gradient-based optimization procedures. To overcome the difficulties arising from the particular minimization problem a moving frame algorithm is applied, cf. [2].

3. Numerical Example

For a demonstration of the applicability of the previously described method we consider a randomly generated microstructure as a target structure, where we are able to calculate virtual experiments as a reference.

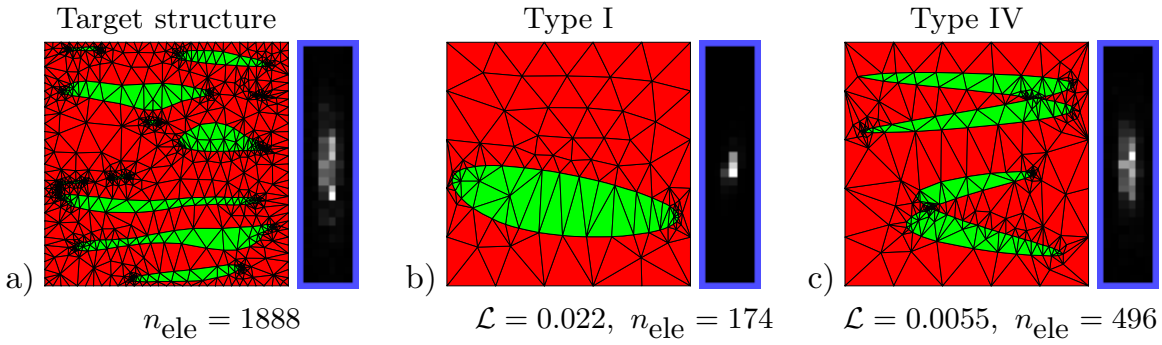

Figure 1. FE-discretizations with relevant spectral densities for the a) target structure and the SSRVE b) type I and c) type IV.

In Fig. 1a the Finite-Element discretization by 1888 triangular elements with quadratic ansatz functions and the relevant area of the spectral density is shown for the chosen target structure. For the generation of the SSRVE we consider four different types of inclusion morphologies: one inclusion with three sampling points (type I) leading to convex inclusions, one inclusion with four sampling points (II) and two inclusions with three (type III) and four (type IV) sampling points each. Then the optimization process is performed and the resulting microstructures for type I and IV are shown in Fig. 1b,c. As can be seen the spectral density of type IV is more similar to the one of the target structure. This is also reflected by the lower value of the objective function $\mathcal{L} = 0.0055$ compared to type I where the value is $\mathcal{L} = 0.022$. This is somehow obvious since the complexity of the microstructure increases for an increasing number of sampling points (degrees of freedom in the objective function). The increasing complexity is also observable by the increasing number of finite elements required for the discretization. In order to study the SSRVEs capability to reflect the mechanical response of the target structure we compare the stress-strain response of the SSRVEs with the response of the target structure in three virtual experiments: tension in i) horizontal and

ii) vertical direction, and iii) shear. Fig. 2 compares the stress-strain curves of the SSRVEs with the target structure.

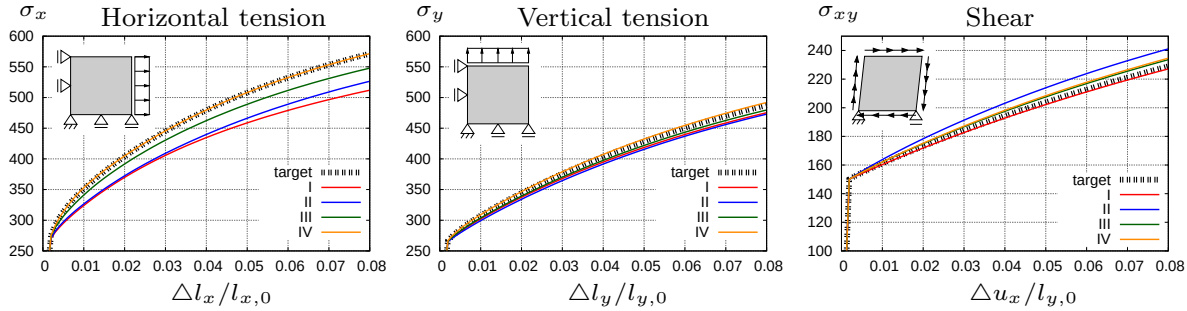

FIGURE 2. Stress-strain response of the target structure and the SSRVE types I to IV for the three virtual experiments.

For the vertical tension test all SSRVEs fit the curve accurately. But for the shear test and especially for the horizontal tension test there is a significant discrepancy between the results of types I, II, III and IV. In addition, we observe a decreasing error for increasing degrees of freedom in the SSRVE generation for the horizontal tension test. Summarizing, type IV leads to the best mechanical results while having the most complex inclusion morphology.

Acknowledgement: The financial support of the "Deutsche Forschungsgemeinschaft" (DFG), project no. SCHR 570-8/1, is gratefully acknowledged.

REFERENCES

[1] D. Balzani and J. Schröder. Some basic ideas for the reconstruction of statistically similar microstructures for multiscale simulations. *Proceedings of Applied Mathematics and Mechanics*, 8:10533–10534, 2008.

[2] D. Balzani and J. Schröder. Reconstruction of statistically similar microstructures for FE^2-simulations in elasto-plasticity. In *Proceedings of the International Symposium of Plasticity 2009*. Neat press,ISBN: 0-9659463-9-8, 2009.

[3] D. Balzani, J. Schröder, and D. Brands. FE^2-simulation of microheterogeneous steels based on statistically similar rve's. In *Proceedings of the IUTAM Symposium on Variational Concepts with applications to the mechanics of materials, September 22-26, 2008, Bochum, Germany*, 2009. in press.

[4] C. Miehe, J. Schröder, and J. Schotte. Computational homogenization analysis in finite plasticity. simulation of texture development in polycrystalline materials. *Computer Methods in Applied Mechanics and Engineering*, 171:387–418, 1999.

[5] G.L. Povirk. Incorporation of microstructural information into models of two-phase materials. *Acta Metallurgica*, 43/8:3199–3206, 1995.

[6] J. Schröder. *Homogenisierungsmethoden der nichtlinearen Kontinuumsmechanik unter Beachtung von Stabilitätsproblemen*. Bericht aus der Forschungsreihe des Institut für Mechanik (Bauwesen), Lehrstuhl I, 2000. Habilitationsschrift.

[7] R.J.M. Smit, W.A.M. Brekelmans, and H.E.H. Meijer. Prediction of the mechanical behavior of nonlinear heterogeneous systems by multi-level finite element modeling. *Computer Methods in Applied Mechanics and Engineering*, 155:181–192, 1998.

Homogenization of elasticity equations without scale separation

Leonid Berlyand

1. Homogenization of elasticity equations without scale separation

In this joint work with H. Owhadi (Caltech), we investigate the homogenization of divergence form elliptic (scalar and vectorial) equations with arbitrary bounded coefficients (in particular, in situations where assumptions of scale separation and/or ergodicity are not satisfied). We prove the existence of an h- basis that is superior to standard piecewise polynomial bases with the same number of degrees of freedom. We obtain an explicit error constant for h-basis approximations, which is independent of the contrast of the material and geometry of its microstructure. We also discuss minimization of the number of "cell" (precomputed) problems for homogenization with arbitrary bounded coefficients and show that this issue is related to a new class of elliptic inequalities. Finally, we will discuss potential applications of this work ranging from brain damage and virtual liver surgery to reservoir modeling and upscaling of atomistic models.

2. Modeling and Analysis of suspensions of active swimmers

This work is devoted to the transition from the well developed modeling and analysis of passive suspensions to active suspensions (namely, bio-suspensions). Modeling of bacterial suspensions and, more generally, of suspensions of active microparticles has recently become an increasingly active area of research. The focus of our work is on the development and analysis of a mathematical PDE model for the multiscale problem of bacterial suspensions. In recent works on the effective viscosity of dilute bacterial suspensions (with Aronson, Haines and Karpeev) explicit formulas have been obtained for the effective viscosity of such suspensions in the limit of small concentrations. These formulas includes the two terms that are found in the Einsteiń classical result for passive suspensions. To this, our main result added an additional term due to self-propulsion (including stochastic tumbling) which depends on the physical and geometric properties of the active suspension. This term explains the experimental observation of a decrease in effective viscosity in active suspensions. We also performed asymptotic analysis of the swimming patterns of bacteria (with Aronson, Gyrya and Karpeev). Here interactions between bacteria are taken into account (unlike in the dilute limit).

Complex Automata: distributing simulations across scales

Alfonso Caiazzo
(joint work with D.Evans, J.L. Falcone, J.Hegewald, E.Lorenz, B.Stahl, D.Wang, J.Bersndorf, B.Chopard, R.Hose, M.Krafczyk, A.G.Hoekstra)

1. Introduction

Complex Automata (CxA) has been recently introduced as a paradigm for multiscale modeling and simulation (see e.g. [1]) The basic idea behind CxA is that a multiscale process can be decomposed into a set of single scale interacting models, each considered as an Automaton, i.e. an independent computational entity communicating with the others.

To build a Complex Auotmata model, a given multiscale system is represented on a **Scale Separation Map** (SSM), a cartesian plane where horizontal and vertical axes represent the temporal and spatial scales. Within this picture a single multiscale algorithm can be drawn as a big box, resolving a wide range of scales, e.g. from micro- to macroscale, and from very fast to very slow processes. The computational approach consists in decomposing this complex system in several *single scale models*, i.e. simpler algorithms, focusing on particular scales (see for example figure 1).

We further restrict these single scale models to have a common evolution loop, considering Cellular Automata, lattice Boltzmann, or Agent Based Models. This assumption is not restrictive, as many physical and biological system can be described with those classes of algorithms.

The relevant achievements of this work can be summarized as follows. Starting from the assumptions on the structure of the single scale models, the theoretical concepts of CxA have been implemented in multiscale coupling library (MUSCLE), a CxA dedicated software environment. This framework will be useful for realizing complex coupling configurations, allowing flexibility in the use of different native codes for the single scale solvers, as well as the necessary software ingredients to implement multiscale coupling templates. From the application point of view, we investigate an original coupled model for in-stent restenosis (a maladaptive response of a blood vessel to injury caused by the deployment of a stent), a biomechanical process modeled by coupling a Lattice Boltzmann model (blood flow), Agent Based model (biological tissue) and a Finite Difference Scheme (drug diffusion). Preliminary simulation results of the CxA setup will be shown.

2. MUSCLE: a multiscale coupling library

The conceptual ideas behind the CxA approach (decomposition in single scale models, restriction to a common instruction flow and specification of finite number of coupling templates) have been used to develop MUSCLE (MUltiscale Coupling Library and Environment, `http://developer.berlios.de/projects/muscle/`) a software environment where a CxA can be implemented naturally [2].

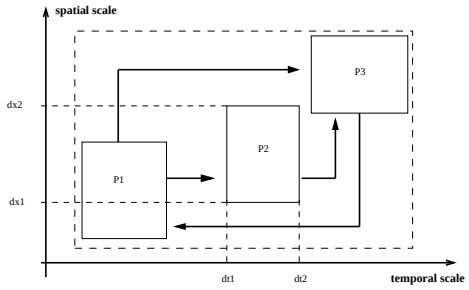

FIGURE 1. Example of SSM: a multiscale process (dashed edges box) has been decomposed in 3 coupled single scale models.

The library is based on JADE (`www.jade.tilab.com`), a multiagent JAVA platform, where both the **kernels** of the simulation (i.e. the single scale models) and the **conduits** (i.e. the coupling templates) are treated as agents.

This allows a complete independence from native codes (and their programming languages), which can be replaced with different sources, provided the interface with respect to the framework remains the same. Furthermore, the fact that coupling interfaces are computational agents allows the implementation of complex communications (smart conduits), where multiscale couplings can be performed.

It is important to remark that the single scale models do not need to be aware of each other, and the information concerning the coupling and the global CxA setup are held by the framework.

In practice, the CxA setup and the use of multiagent coupling library realizes a natural distribution of the computational work among the different scales.

In the particular application described below, we implement the mutual coupling of three single scale models written in FORTRAN90, C++ and JAVA.

3. A Multiscale model for in-stent restenosis

A *stenosis* is a narrowing of a blood vessel lumen due to the presence of an atherosclerotic plaque. This can be corrected by balloon angioplasty, after which a *stent* (metal mesh) is deployed to prevent the vessel from collapsing. The injury caused by the stent can lead to a maladaptive biological response of the cellular tissue (mainly smooth muscle cells). The abnormal growth can produce a new stenosis (re-stenosis). Additionally, stents may be coated with active compounds which, can prevent proliferation of smooth muscle cells and neointimal growth (see [3] for a more complete discussion on the multiscience and multiscale nature of in-stent restenosis).

We describe, showing preliminary simulation results, a simplified two dimensional CxA setup for in-stent restenosis, coupling a *lattice Boltzmann* blood flow (BF) solver, an *agent based model* for the Smooth Muscle Cells (SMC) dynamics and a *Finite Difference scheme* for the Drug Diffusion (DD) within the cellular tissue [4] .

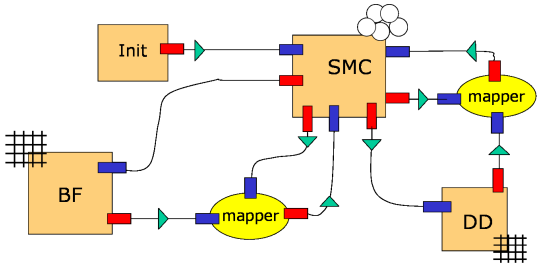

FIGURE 2. The Connection Scheme, showing the single scale models (BF, SMC, DD), the Initialization agent, and the conduits connectivity. For each single scale models it is specified whether it is mesh-based (BF, DD) or Agent-based (SMC).

Coupling Relations. The BF is the fastest process (periodic, time scale of $O(s)$). It is approximated via an incompressible fluid, undergoing a periodic pulse (with 1-second period), whose domain needs to be updated after each changes in smooth muscle cells configuration. The DD process is modeled solving an anisotropic diffusion equation, with an intermediate time scale (diffusion of common drugs relaxes to steady state in $O(h)$), with a FD scheme. As for the BF, the diffusion domain (the cellular tissue) needs to be updated according to the cell geometry. SMCs (time scale of cell cycle is of the order of 1 day) are modeled using an Agent Based solver, where each single cell is an agent, able to react to physical forces exerted by other agents, and evolving according to a set of biological rules, which governs cell proliferation. Through these rules, depending on fluid stresses near the vessel boundary and on drug concentration within the tissue, the agents are coupled to the rest of the model (figure 2).

Acknowledgements. This research is supported by the European Commission, through the COAST project (`www.complex-automata.org`, EU-FP6-IST-FET Contract 033664). Alfonso Caiazzo is supported by an ERCIM " Alain Bensoussan " fellowship programme.

REFERENCES

[1] A.G. Hoekstra, E. Lorenz, J.L. Falcone, B. Chopard, *Towards a Complex Automata Formalism for Multi-Scale Modeling*, Int. J. Mult. Comp. Eng., **5** (2007), 491–502.

[2] J. Hegewald, M. Krafczyk, J. Tölke, A.G. Hoekstra, B. Chopard, B. *An Agent-Based Coupling Platform for Complex Automata*. Lecture Notes in Computer Science 5102 (2008), 227–233.

[3] D. Evans, P. Lawford, J. Gunn, D. Walker, R. Hose, R. Smallwood, B. Chopard, M. Krafczyk, J. Bernsdorf, A. Hoekstra, *The application of multiscale modelling to the process of development and prevention of stenosis in a stented coronary artery*, Phil. Trans. Roy. Soc. A, **366** (2008), 3343–3360.

[4] A. Caiazzo, D. Evans, J.L.. Falcone, J. Hegewald, E. Lorenz,B. Stahl, D. Wang, J. Bernsdorf, B. Chopard, J. Gunn, R. Hose, M. Krafczyk, P. Lawford, R. Smallwood, D. Walker, A.G. Hoekstra, *Towards a Complex Automata Multiscale Model of In-stent Restenosis*, submitted (2009).

A fully discrete scheme for the computation of microstructures in solids

Georg Dolzmann
(joint work with Sergio Conti)

The computation of microstructures in solids is a challenging problem at the interface between mathematical analysis, algorithmic and numerical methods, and materials science. Even the characterization of stationary states is a subtle issue since they frequently do not exist in a classical sense. The fundamental obstacle is a lack of convexity of the free energy density and correspondingly a failure of weak lower semi-continuity of the variational integrals. In such a situation one typically observes that minimizing sequences develop oscillations at finer and finer scales. The weak limit is not a minimizer of the variational problem, but the gradient Young measure associated to the sequence of deformation gradients captures the correct statistical information about the oscillations in the minimizing sequence.

In this talk we propose a fully discrete scheme based on the computation of an approximation to the relaxed energy density and the minimization of the relaxed functional; for semi-discrete schemes see [1]. More precisely, we let

$$I[u] = \int_\Omega W(Du)\mathrm{d}x\,, \qquad I^{\mathrm{qc}}[u] = \int_\Omega W^{\mathrm{qc}}(Du)\mathrm{d}x$$

where W^{qc} is the quasiconvex envelope of the energy density W, see [4] for the relations between I and I^{qc}. Only in exceptional cases a closed formula for W^{qc} has been derived and hence the macroscopic properties of the solution of the elasticity problem cannot be computed numerically by simply resorting to the relaxed variational problem I^{qc}. Therefore we propose a novel algorithm for the concurrent computation of the relaxed energy density W^{qc} and a finite element minimizer u_h. In order to focus on the aspects concerning the approximation of the relaxed problem we assume that the finite element scheme is based on Courant elements (piecewise affine and continuous) on a regular triangulation.

The fundamental approximation step consists of seeking a first order laminate with center of mass equal to F for the approximation of

$$W^{\mathrm{qc}}(F) \sim W^{(1)}(F) = \inf_{\lambda,a,n} \left[\lambda W\big(F + (\lambda-1)a\otimes n\big) + (1-\lambda)W\big(F+\lambda a\otimes n\big)\right].$$

Formally, the laminate can be written as a probability measure

$$\nu = \lambda\delta_{F+(\lambda-1)a\otimes n} + (1-\lambda)\delta_{F+\lambda a\otimes n} \tag{1}$$

where $\lambda\in[0,1]$, $a\in\mathbb{R}^2$ and $n\in\mathbb{S}^1$ describe the four free parameters for a simple laminate in 2×2 matrices. For simplicity we assume here that $n=m=2$, the generalization to arbitrary dimensions is straightforward.

Our numerical scheme is based on two design principles:

(a) The relaxed energies that are explicitly known in the literature share the common feature that the formulas giving the relaxed energies via a laminate of first or second order change smoothly in F and the characteristic features (e.g. the change from a first order laminate to a second order laminate) happen across

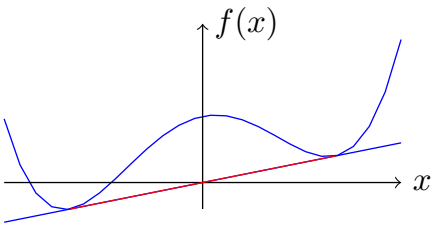

FIGURE 1. Typical situation in the convexification along a rank-one line: the graph has convex and concave parts. In this case, the convexification agrees between the two (local) minima of f with the affine supporting function. This is indicated by the red segment on this line.

certain hypersurfaces. This suggests that a laminate at a given point F should provide us with a good initial value for the computation of a laminate at a point $F + \Delta F$ with ΔF small.

(b) If we consider the energy W along a rank-one line, then there are typically three distinct regions in which the energy is (i) convex and agrees with the convex envelope along this line, is (ii) convex but does not agree with the convex envelope along this line, is (iii) concave, see Figure 1. In the concave regions, the energy is typically significantly larger than the convexification along this line and an optimization scheme will lead to a good result. On the other hand, in convex regions where the energy does not agree with the convex envelope, the difference between these two energies can be quadratically small and optimization algorithms might not be able to detect this difference. This fact motivates to include in the algorithmic strategy steps in which information about microstructure is shared on a more global and less local scale.

The approximation of $W^{(1)}$ is based on a discretization of a box $[-L, L]^{m\times n}$ in the space of all deformation gradients. Note that most of the physically relevant energies are frame indifferent, that is, $W(F) = W(QF)$ for all $Q \in \mathrm{SO}(n)$. Hence one only needs to store the symmetric part U of a given deformation gradient. This discretization is realized as a tree $\mathcal{T}$ which is initialized at the center of the box with a corresponding microstructure. Each node in $\mathcal{T}$ contains four values describing a laminate and 2^{mn} pointers to the subcubes that one obtains with a dyadic decomposition of the given cube into 2^{mn} congruent ones with half the length of the one-dimensional edges. Fix a parameter $\epsilon > 0$.

ALGORITHM: *Computation of* $W^{\mathrm{qc}}(F)$ *and* $DW^{\mathrm{qc}}(F)$*:*

(1) locate the smallest box within $\mathcal{T}$ that contains F; let Z be it's center;
(2) if $|F - Z| < \epsilon$, use the laminate at Z as an initial value for an optimization scheme for the minimization over first order laminates at F represented as in (1) and return

$$W^{\mathrm{qc}}(F) \sim \int_{\mathbb{M}^{m\times n}} W(A)\mathrm{d}\nu(A)\,, \quad DW^{\mathrm{qc}}(F) \sim \int_{\mathbb{M}^{m\times n}} DW(A)\mathrm{d}\nu(A)\,;$$

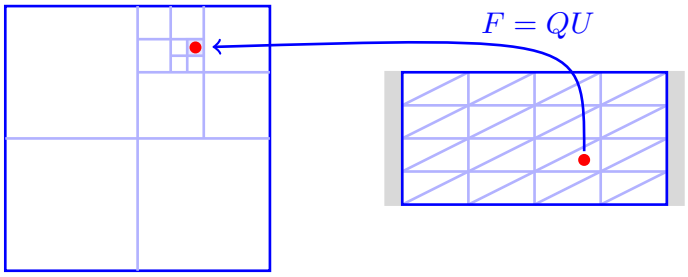

FIGURE 2. Sketch of the discretization in matrix space for $W^{(1)}$ and in Ω for the deformation u_h in a finite element space.

(3) if $|F - Z| > \epsilon$, divide the cube into 2^{mn} congruent subcubes, compute a laminate at the center of the subcube containing F and return to Step 1.

Depending on a global criterion, e.g., a certain number of evaluations of the approximation of the energy or after a certain number of iterations in the global minimization for the elasticity problem, one performs at least once and possible multiple times a global tree improvement step:

(4) for all children in $\mathcal{T}$ minimize over first order laminates with all the laminates from neighboring cubes as initial values and pick the optimal one giving the smallest energy as the new approximation on this cube.

Remarks: (a) This scheme clearly separates the discretization in the finite element method and the discretization in matrix space. Consequently, the scheme can be used on a parallel computer.

(b) The global improvement step (4) can be implemented in several ways. One option is to proceed in the spirit of a multigrid method and use the hierarchical structure of the dyadic cubes to realize the propagation of information on a more global basis.

(c) Good benchmark examples are the energy density related to nematic elastomers in [2] for which an explicit formula is known or the energy densities in [3] which demonstrate the subtle dependence on constraints like incompressibility.

(d) Higher order laminates at a given point F can be realized by recursively substituting first order laminates for all matrices in the support of the laminate stored at F.

(e) The tree $\mathcal{T}$ is typically sparse since only those subtrees are generated that contain deformation gradients needed in the solution of the elasticity problem.

REFERENCES

[1] C. Carstensen, S. Conti, A. Orlando, *Mixed analytical-numerical relaxation in finite single-slip crystal plasticity*, Cont. Mech. Thermod. **20** (2008), 275-301.

[2] S. Conti, A. DeSimone, G. Dolzmann, *Semi-soft elasticity and director reorientation in stretched sheets of nematic elastomers*, Phys. Rev. E **66** (2002), #061710.

[3] S. Conti, G. Dolzmann, C. Klust, *Relaxation of a class of variational models in crystal plasticity*, Proc. Roy. Soc. London A **465** (2009), 1735-1742.

[4] B. Dacorogna, *Direct methods in the calculus of variations*, Applied Mathematical Sciences **78**, Springer, Berlin, 1989.

Multiscale Methods for Hydrodynamics of Polymer Chains in Solution

Aleksandar Donev

The hydrodynamics of complex fluids, such as polymer solutions and colloidal suspensions, has attracted great interest due to recent advances in fabrication of micro- and nano-fluidic devices. I will first review recent advances in mesoscopic numerical methods for simulating the interaction between complex fluid flow and suspended macro molecules and structures. Computational issues at play include coarse-graining to bridge the large gap in timescales and length scales, coupling between disparate methods such as molecular dynamics and Navier-Stokes solvers, the inclusion of thermal fluctuations.

I will then present my recent work at LLNL to develop novel particle methods for modeling polymer chains in flow. Typically, Molecular Dynamics (MD) is used for the polymer chains, and the solvent is modeled with a mesoscopic method. In our algorithm, termed Stochastic Event-Driven Molecular Dynamics (SEDMD) [A. Donev and A. L. Garcia and B. J. Alder, J. Comp. Phys., 227(4), 2644-2665, 2008], polymers are modeled as chains of hard spheres and the solvent is modeled using a dense-fluid generalization of the Direct Simulation Monte Carlo (DSMC) method [Phys. Rev. Lett., 101, 075902, 2008]. Even with all of the speedup compared to brute-force MD the algorithm is still time-consuming due to the large number of solvent particles necessary to fill the computational domain. It is natural to restrict the particle model only to regions close to a polymer chain and use a lower-resolution continuum model elsewhere. I will present a hybrid method that couples an explicit fluctuating compressible Navier-Stokes solver with the particle method. The coupling is flux-based and generalizes previous work [J. B. Bell and A. L. Garcia and S. A. Williams, SIAM Multiscale Modeling and Simulation, 6, 1256-1280, 2008] to dense fluids as appropriate for polymer problems.

I will conclude with a look into the challenges of developing a simulation methodology capable of simulating macroscopic flows of complex fluids with atomistic fidelity.

The partial evaluation of the inverse and its relation to multi-scale problems

Wolfgang Hackbusch

Consider a boundary value problem with the partial differential equation

$$\mathcal{L}u = f \quad \text{in } \Omega \quad \text{with } \mathcal{L} = \mathrm{div} a(\cdot) \mathrm{grad}$$

and for instance Dirichlet boundary data $u|_\Gamma = g$. A fine scale behaviour may be caused by an oscillatory coefficient $a(\cdot)$ or by a complicated structure of Ω. In the following we assume that there is a *fine grid size* h such that the details of $a(\cdot)$ and / or Ω and consequently of the solution u can be resolved by a discretisation with this grid size h. On the other hand, in most of the applications one is not interested in the solution with all its details. Instead one is looking for the meso-scale behaviour,

i.e., for the (averaged) solution for a *meso-scale grid size* H ($h \ll H \ll 1$) or one likes to know several local functionals of the solution.

The classical homogenisation method [1] starts from the operator $\mathcal{L}$ and assuming periodic fine-scale behaviour with a period of size ε it produces a homogenised operator $\mathcal{L}^{\hom}$ with constant coefficients. Hence, $\mathcal{L}^{\hom}$ can easily be used for a discretisation $L_H^{\hom}$ with a certain grid size H :

$$\begin{array}{ccccccc} & & & & \mathcal{L}^{\hom} & \to & L_H \quad \to \quad u_H := (L_H)^{-1} f_H \\ (1) & & & \nearrow & & & \\ & \mathcal{L} & \to & L_h^{\mathrm{cell}} & & & \end{array}$$

Note that the computation of the homogenised coefficients of $\mathcal{L}^{\hom}$ is usually done numerically by solving cell problems with step size $h < \varepsilon$. The overall error of the discrete solution depends on ε (homogenisation error) and H (usual discretisation error).

In the following we consider the case of a fine-scale behaviour without periodic structure. A prototype of a solution strategy in this situation is due to T. Hou ([3]),([4]). He proposes a finite element method in a grid of the meso-scale H from above, but the finite element basis functions b_i are (ideally) homogeneous solutions, i.e. $\mathcal{L}b_i = 0$ in each triangle. Practically, in each triangle one has to solve boundary value problems by means of a discretisation using a fine grid size $h \ll H$. Although the fine scale discretisation L_h of the following diagram is used only locally, the cost for generating the basis functions b_i is at least $O(N_h)$, where N_h denotes the dimension of the finite element method in the fine grid of size h.

$$\begin{array}{ccccccc} & & & & L_H & \to & u_H := (L_H)^{-1} f_H \\ (2) & & & \nearrow & & & \\ & \mathcal{L} & \to & L_h & & & \end{array}$$

The overall error depends in a special way of both step sizes h and H.

The common property of the approaches (1) and (2) is that they use the fine-scale discretisation L_h only locally. The introduction of L_H produces a further discretisation error depending of H. The inversion process is done in the end when the discrete problem $L_H u_H = f_H$ is solved.

Our approach starts again with the fine grid discretisation $\mathcal{L} \to L_h$, but the transition to the meso-scale H is performed on the basis of the inverse matrix L_h^{-1} :

$$\begin{array}{ccccccc} & & & & \Pi_{2,H} L_h^{-1} \Pi_{1,H}^* = \text{“}\, L_H^{-1} \,\text{”} \\ (3) & & & \nearrow & \uparrow \\ & \mathcal{L} & \to & L_h & \to & L_h^{-1} \end{array}$$

Formally one can think of projecting $L_h^{-1} : V_h' \to V_h$ (V_h: finite element space corresponding to h) into $\Pi_{2,H} L_h^{-1} \Pi_{1,H}^* : V_H' \to V_H$ where $\Pi_{i,H} : V_h \to V_H$ ($i = 1, 2$) are the mappings (e.g., projections) of the fine-scale finite element space V_h into the meso-scale finite element space $V_H \subset V_h$. The underlying algorithm does

not perform the two steps $L_h \to L_h^{-1} \to \Pi_{2,H} L_h^{-1} \Pi_{1,H}^*$, but approximates the map $L_h \to \Pi_{2,H} L_h^{-1} \Pi_{1,H}^*$ indirectly.

If $\Pi_{1,H} = \Pi_{2,H}$ is the interpolation in the coarse-grid nodal points of V_H, the matrix $\Pi_{2,H} L_h^{-1} \Pi_{1,H}^*$ is of size $N_H \times N_H$ ($N_H = \dim V_H$) and coincides with L_h^{-1} restricted to the row and columns corresponding to the V_H nodal points. Hence, $\Pi_{2,H} L_h^{-1} \Pi_{1,H}^*$ realised a *partial evaluation* of the inverse L_h^{-1}. If I_h describes the index set of all V_h nodal points and $I_H \subset I_h$ those of V_H, another notation of $\Pi_{2,H} L_h^{-1} \Pi_{1,H}^*$ is $\left(L_{h,i,j}^{-1}\right)_{i,j \in I_H}$.

The numerical algorithm and its cost are explained in detail in Chapter 12 of [2]. In fact, the algorithms yields not only $\left(L_{h,i,j}^{-1}\right)_{i,j \in I_H}$ from above but $\left(L_{h,i,j}^{-1}\right)_{i,j \in I_{H,h}}$, where $I_{H,h}$ contains all nodal points lying on the boundaries of the triangles of the V_H-finite elements. Differently from (1) and (2), the algorithm directly yields the *solution mapping* from (f, g), $f \in V_H$ right-hand side, g boundary data on Γ, to the restriction $(u_{h,i})_{i \in I_{H,h}}$ of the fine-scale solution $u_h = L_h^{-1} f$. Therefore, the choice of H does not introduce any new discretisation error. On the hand, the method does *not* yield a coarse-grid model L_H. One may view $\Pi_{2,H} L_h^{-1} \Pi_{1,H}^*$ as the inverse of L_H as indicated by the quotation marks in (3). However, then $L_H := \left(\Pi_{2,H} L_h^{-1} \Pi_{1,H}^*\right)^{-1}$ is a fully populated matrix and not a sparse finite element matrix. One may ask

- whether there is a sparse $\widetilde{L_H}$ such that $\Pi_{2,H} L_h^{-1} \Pi_{1,H}^*$ and $\left(\widetilde{L_H}\right)^{-1}$ coincide up to $O(H^\sigma)$ (σ: suitable consistency order) in a suitable norm
- or whether there is "homogenised" pde such that the corresponding finite element discretisation $\widetilde{L_H}$ has the property from above.

To formulate a precise analytic question, one should send h to 0. Then L_h^{-1} becomes $\mathcal{L}^{-1}$ and $\Pi_{2,H} L_h^{-1} \Pi_{1,H}^*$ becomes the V_H-Galerkin discretisation of the integral operator $\mathcal{K} f(x) := \int_\Omega g(x,y) f(y) \mathrm{d}y$, where g is the exact Green function of $\mathcal{L}$.

References

[1] A. Bensoussan, J-L. Lions, and G. Papanicolaou: Asymptotic analysis for periodic structures. Studies in Mathematics and its Applications, vol. 5. North-Holland Publishing Co., Amsterdam, 1978.

[2] W. Hackbusch: Hierarchische Matrizen - Algorithmen und Analysis. ISBN 978-3-642-00221-2. Springer Dordrecht, Heidelberg, London, New York. 2009.

[3] T. Y. Hou and X.-H. Wu: A multiscale finite element method for elliptic problems in composite materials and porous media. J. Comput. Phys., **134**:169–189, 1997.

[4] T. Y. Hou, X-H. Wu, and Z. Cai: Convergence of a multiscale finite element method for elliptic problems with rapidly oscillating coefficients. Math. Comp. **68**(227):913–943, 1999.

[5] A.G. Litvinenko: Application of hierarchical matrices for solving multiscale problems. Doctoral thesis, Universität Leipzig, 2007.

Multiscale modeling of shape memory alloys

Klaus Hackl

Shape memory alloys posses a natural multiscale structure, starting from different lattice geometries for the various phases at the atomic scale, continuing with the specific martensitic microstructures at the microscale up to the polycrystalline aggregate at the mesoscale. We suggest here a model considering all scales in a uniform way, based on energetic considerations.

We investigate inelastic materials described by so-called internal or history-variables. Examples include elastoplastic but also damaged materials or those undergoing phase-transformations. By investigating associated potentials in a time-incremental setting it is possible to model the onset of the formation of microstructures but not their subsequent evolution, [3, 5, 11, 12, 13]. Here, some general ideas will be presented on how this problem could be treated.

In an isothermal setting and for infinitesimal strains the state of a general inelastic material will be defined by its strain tensor $\boldsymbol{\varepsilon} = 1/2(\nabla \boldsymbol{u} + \nabla \boldsymbol{u}^{\mathrm{T}})$ and a collection of internal variables: $\boldsymbol{K}$. Denoting the specific Helmholtz free energy by $\Psi(\boldsymbol{\varepsilon}, \boldsymbol{K})$ we introduce thermodynamically conjugate stresses by $\boldsymbol{\sigma} = \frac{\partial \Psi}{\partial \boldsymbol{\varepsilon}}$, $\boldsymbol{Q} = -\frac{\partial \Psi}{\partial \boldsymbol{K}}$. The evolution of $\boldsymbol{K}$ is then governed either by a so-called inelastic potential $J(\boldsymbol{K}, \boldsymbol{Q})$ or its Legendre-transform, the dissipation functional: $\Delta(\boldsymbol{K}, \dot{\boldsymbol{K}}) = \sup \left\{ \dot{\boldsymbol{K}} : \boldsymbol{Q} - J(\boldsymbol{K}, \boldsymbol{Q}) \,\middle|\, \boldsymbol{Q} \right\}$. The evolution equations are then given in the two equivalent forms

$$\dot{\boldsymbol{K}} \in \frac{\partial J}{\partial \boldsymbol{Q}}, \qquad \boldsymbol{Q} \in \frac{\partial \Delta}{\partial \dot{\boldsymbol{K}}}. \tag{1}$$

The entire evolution problem can now be described in terms of two minimum principles, where we follow ideas presented in [4, 10, 13]. Considering the Gibbs free energy of the entire body $\mathcal{I}(t, \boldsymbol{u}, \boldsymbol{K}) = \displaystyle\int_\Omega \Psi(\nabla \boldsymbol{u}, \boldsymbol{K}) \,\mathrm{d}V - \ell(t, \boldsymbol{u})$ the deformation is given by the principle of minimum potential energy:

$$\boldsymbol{u} = \operatorname{argmin} \left\{ \mathcal{I}(t, \boldsymbol{u}, \boldsymbol{K}) \,\middle|\, \boldsymbol{u} = \boldsymbol{u}_0 \text{ on } \Gamma_u \right\}. \tag{2}$$

Here Ω is the material body, Γ_u a subset of its boundary and $\ell(t, \boldsymbol{u})$ the potential of external forces. On the other hand introducing the Lagrange functional $\mathcal{L}(\boldsymbol{u}, \boldsymbol{K}, \dot{\boldsymbol{K}}) = \dfrac{d}{dt} \Psi(\nabla \boldsymbol{u}, \boldsymbol{K}) + \Delta(\boldsymbol{K}, \dot{\boldsymbol{K}})$ we can write the evolution equation (1) in the form

$$\dot{\boldsymbol{K}} = \operatorname{argmin} \left\{ \mathcal{L}(\boldsymbol{u}, \boldsymbol{K}, \dot{\boldsymbol{K}}) \,\middle|\, \dot{\boldsymbol{K}} \right\}. \tag{3}$$

At the level of single crystals we use a partially relaxed energy derived via a laminate of second order, see [1, 2]. In this sense, the displacement-field on the microscale $\mathbf{u} = \mathbf{u}^{\mathrm{hom}} + \mathbf{u}^{\mathrm{pert}}$ is decomposed into a homogeneous part $\mathbf{u}^{\mathrm{hom}} = \boldsymbol{\varepsilon} \cdot \mathbf{x}$ and a perturbation-field $\mathbf{u}^{\mathrm{pert}}$. These perturbations can be mathematically

expressed by

$$\mathbf{u}_{1st}^{pert} = \begin{cases} \mathbf{u}_A^{pert} = \frac{1}{\lambda_A}\,\mathbf{u}_A\;(\xi - i + 1) & ,\text{if } i-1 \le \xi \le i-1+\lambda_A \\ \mathbf{u}_M^{pert} = -\frac{1}{\lambda_M}\,\mathbf{u}_A\;(\xi - i) & ,\text{else} \end{cases} \tag{4}$$

and

$$\mathbf{u}_I^{pert} = \mathbf{u}_M^{pert} + \frac{1}{\lambda_I}\,(\mathbf{u}_I - \mathbf{u}_{I-1})\left(\mathbf{x}\cdot\mathbf{n}_M - \sum_{k=1}^{I-1}\{\lambda_k\} - (j-1)\lambda_M\right) + \mathbf{u}_{I-1} \tag{5}$$

$$\mathbf{u}_{2nd}^{pert} = \begin{cases} \mathbf{u}_1^{pert} & ,\text{if } i-1+\lambda_A \le \xi \le i \;\wedge\; j-1 \le \zeta \le j-1+\lambda_1 \\ \mathbf{u}_2^{pert} & ,\text{if } i-1+\lambda_A \le \xi \le i \;\wedge\; j-1+\lambda_1 \le \zeta \le j-1+\lambda_1+\lambda_2 \\ \vdots & \\ 0 & ,\text{else} \end{cases} \tag{6}$$

where $i = 1, 2, \ldots$ and $j = 1, 2, \ldots$ denote the current periodic pattern of 1st order and second order laminates, respectively. This results in an overall perturbation-field $\mathbf{u}^{pert} = \mathbf{u}_{1st}^{pert} + \mathbf{u}_{2nd}^{pert}$. In a straight forward way one obtains

$$\boldsymbol{\varepsilon}_A = \boldsymbol{\varepsilon} + \frac{1}{\lambda_A}\,\mathbf{n}_A \otimes_S \mathbf{u}_A \tag{7}$$

$$\boldsymbol{\varepsilon}_I = \boldsymbol{\varepsilon} - \frac{1}{\lambda_M}\,\mathbf{n}_A \otimes_S \mathbf{u}_A + \frac{1}{\lambda_I}\,\mathbf{n}_M \otimes_S (\mathbf{u}_I - \mathbf{u}_{I-1}) \quad ,I = 1 \ldots NV \tag{8}$$

with $\mathbf{a} \otimes_S \mathbf{b} = \frac{1}{2}\,(\mathbf{a}\otimes\mathbf{b} + \mathbf{b}\otimes\mathbf{a})$, $\mathbf{u}_0 = \mathbf{0}$, $\mathbf{u}_{NV} = \mathbf{0}$ as strain-states within each phase-domain.

Here the volume fractions of each martensite-variant λ_I along with $\lambda_A = (1 - \lambda_M)$, $\lambda_M = \sum_{I=1}^{NV} \lambda_I$ as overall portions of austenite/martensite have been introduced.

Obviously, the perturbed displacement-field is incompatible at the phase-interfaces. At this point, however, we assume that the lengthscale of higher order laminates is infinitely small compared to the one of lower order. Now, compatibility is satisfied in an averaged sense due to the fact that

$$\int_{\mathcal{RVE}} \boldsymbol{\varepsilon}\,(\mathbf{x})\;dV = \lambda_A\,\boldsymbol{\varepsilon}_A + \sum_{I=1}^{NV} \lambda_I\,\boldsymbol{\varepsilon}_I = \boldsymbol{\varepsilon} \tag{9}$$

holds. With these definitions at hand, the relaxed energy-density can be written as

$$\begin{aligned} \psi = {} & \tfrac{1}{2}\boldsymbol{\varepsilon} : \bar{\mathbf{C}} : \boldsymbol{\varepsilon} + \boldsymbol{\varepsilon} : [(\Delta\mathbf{C}\cdot\mathbf{n}_A)\cdot\mathbf{u}_A] + \tfrac{1}{2}\mathbf{u}_A\cdot\hat{\mathbf{C}}\cdot\mathbf{u}_A - \bar{\boldsymbol{\tau}} : \boldsymbol{\varepsilon} \\ & + \tfrac{1}{\lambda_M}\,(\bar{\boldsymbol{\tau}}.\mathbf{n}_A)\cdot\mathbf{u}_A + \bar{\mathcal{C}} + \sum_{I=1}^{NV}\left\{\tfrac{1}{2\,\lambda_I}\,(\mathbf{u}_I - \mathbf{u}_{I-1})\cdot\hat{\mathbf{C}}_M\cdot(\mathbf{u}_I - \mathbf{u}_{I-1})\right\} \\ & - \sum_{I=1}^{NV}\{\boldsymbol{\tau}_I\cdot(\mathbf{u}_I - \mathbf{u}_{I-1})\}\cdot\mathbf{n}_M, \end{aligned} \tag{10}$$

where $\bar{\mathbf{C}} = \lambda_A \mathbf{C}_A + \lambda_M \mathbf{C}_M$, $\Delta\mathbf{C} = \mathbf{C}_A - \mathbf{C}_M$, $\tilde{\mathbf{C}} = \frac{1}{\lambda_A}\mathbf{C}_A + \frac{1}{\lambda_M}\mathbf{C}_M$, $\hat{\mathbf{C}} = \mathbf{n}_A \cdot \tilde{\mathbf{C}} \cdot \mathbf{n}_A = n_{A,i}\,\tilde{C}_{ijkl}\,n_{A,l}\,\mathbf{e}_j\,\mathbf{e}_k$, $\hat{\mathbf{C}}_M = \mathbf{n}_M \cdot \mathbf{C}_M \cdot \mathbf{n}_M = n_{M,i}\,C_{M,ijkl}\,n_{M,l}\,\mathbf{e}_j\,\mathbf{e}_k$, $\bar{\boldsymbol{\tau}} = \sum_{I=1}^{NV} \lambda_I\,\boldsymbol{\tau}_I$, $\bar{\mathcal{C}} = \lambda_A\,\mathcal{C}_A + \lambda_M\,\mathcal{C}_M + \frac{1}{2}\sum_{I=1}^{NV}\lambda_I\,\boldsymbol{\tau}_I : \boldsymbol{\varepsilon}_I^t$ are used as abbreviations.

Let us generalize the concept introduced now to the polycrystalline case, following [9, 7, 8]. An ideal polycrystal will consist of an infinite number of crystallites. In order to obtain a mathematically more concise and numerically manageable formulation, we discretize the Young measure over SO_3 using a large, but finite number N of orientations $\boldsymbol{R}^i$ to be chosen randomly and uniformly distributed in SO_3. Consequently, $\xi^i = \xi\left(\boldsymbol{R}^i, \boldsymbol{x}\right)$ gives the volume fractions of the crystals with orientation i. This measure is then normalized such that $\sum_{i=1}^{N}\xi^i = 1$.

The rotated transformation strain for the jth variant of crystal i yields

$$\boldsymbol{\eta}_t^{ij} = \left(\boldsymbol{R}^i\right)^T \cdot \boldsymbol{\eta}_t^j \cdot \boldsymbol{R}^i \tag{11}$$

and the elasticity tensor for each orientation may be calculated from

$$\mathbb{C}^{ij}_{pqrs} = R^i_{tp} R^i_{uq} R^i_{vr} R^i_{ws} \mathbb{C}^j_{tuvw}\,. \tag{12}$$

Altogether, the energy density of the jth variant within the ith crystal reads

$$\Psi^{ij}\left(\boldsymbol{\varepsilon}^{ij}, \boldsymbol{\eta}_t^{ij}\right) = \frac{1}{2}\left(\boldsymbol{\varepsilon}^{ij} - \boldsymbol{\eta}_t^{ij}\right) : \mathbb{C}^{ij} : \left(\boldsymbol{\varepsilon}^{ij} - \boldsymbol{\eta}_t^{ij}\right) + \alpha^j\,. \tag{13}$$

The volume fraction corresponding to this variant within the corresponding crystallite is now denoted as λ^{ij}. Consequently, mass conservation of each crystal may be formulated as

$$\sum_{j=0}^{n} \lambda^{ij} = 1 \quad \text{for } i = 1, \ldots, N \tag{14}$$

and averaging the strains of all variants for all crystal orientations gives the macroscopical strain

$$\boldsymbol{\varepsilon} = \sum_{i=1}^{N}\sum_{j=0}^{n} \xi^i \lambda^{ij} \boldsymbol{\varepsilon}^{ij}. \tag{15}$$

The characteristic flexibility in the material behavior of shape memory alloys can be explained by their ability to spontaneously transform inbetween austenite and the different martensitic variants. In a polycrystalline alloy, this effect may lead to a microstructure of different strains within the different variants and crystal orientations. The capability of the material to adjust the strains in order to minimize its specific free energy is mathematically formulated as the relaxation of the energy for fixed volume fractions $\boldsymbol{\lambda}$

$$\Psi^{rel}(\boldsymbol{\varepsilon}, \boldsymbol{\lambda}) = \inf_{\boldsymbol{\varepsilon}^{ij}} \left\{ \sum_{i=1}^{N}\sum_{j=0}^{n} \xi^i \lambda^{ij} \Psi^{ij}\left(\boldsymbol{\varepsilon}^{ij}, \boldsymbol{\eta}_t^{ij}\right) \,\middle|\, \boldsymbol{\varepsilon} = \sum_{i=1}^{N}\sum_{j=0}^{n} \xi^i \lambda^{ij} \boldsymbol{\varepsilon}^{ij} \right\}\,. \tag{16}$$

As dissipation functional we choose

$$\Delta(\dot{\boldsymbol{\lambda}}, |\boldsymbol{\lambda}_0|) = r(\boldsymbol{\lambda}_0)\sqrt{\sum_{j=1}^{N} \xi^j \sum_{i=0}^{n} (\dot{\lambda}_i^j)^2}, \tag{17}$$

with

$$|\boldsymbol{\lambda}_0| = \sum_{j=1}^{N} \xi^j \lambda_0^j, \tag{18}$$

with $r(\boldsymbol{\lambda}_0) > 0$. Simulation results untilizing this approach can be found in [1, 2].

References

[1] T. Bartel, K. Hackl, *A novel approach to the modelling of single-crystalline materials undergoing martensitic phase-transformations*, Materials Science and Engineering: A, **481-482** (2008) 371-375.

[2] T. Bartel, K. Hackl, *A micromechanical model for martensitic phase-transformations in shape-memory alloys based on energy-relaxation*, ZAMM, **89** (2009) 792809.

[3] S. Bartels, C. Carstensen, K. Hackl, U. Hoppe, *Effective relaxation for microstructures simulations: algorithms and applications*, Comp. Meth. Appl. Meth. Eng. **193, No. 48-51** (2004) 5143–5175.

[4] C. Carstensen, K. Hackl, A. Mielke, *Nonconvex potentials and microstructures in finite-strain plasticity*, Proc. R. Soc. Lond. A, **458, 2018** (2002) 299–317.

[5] S. Conti, F. Theil, *Single-Slip Elastoplastic Microstructures*, Arch. Rat. Mech. Anal. **178** (2005) 125–148.

[6] S. Govindjee, K. Hackl, R. Heinen, *An Upper Bound to the Free Energy of Mixing by Twin-Compatible Lamination for n-variant Martensitic Phase Transformations*, Contin. Mech. Thermodyn. **18 (7-8)** (2007) 443-453.

[7] K. Hackl, R. Heinen, *A micromechanical model for pretextured polycrystalline shape-memory alloys including elastic anisotropy.* Contin. Mech. Thermodyn. **19 (8)** (2008) 499-510.

[8] K. Hackl, R. Heinen, *An upper bound to the free energy of n-variant polycrystalline shape memory alloys.* J. Mech. Phys. Solids 56 **9** (2008) 2832-2843.

[9] K. Hackl, M. Schmidt-Baldassari, W. Zhang, *A micromechanical model for polycrystalline shape-memory alloys*, Materials Science and Engineering A **378** (2003) 503–506.

[10] A. Mielke, *Finite elastoplasticity, Lie groups and geodesics on SL(d)*, In "Geometry, Dynamics, and Mechanics, P. Newton, A. Weinstein, P. Holmes (eds), Springer–Verlag"(2002) 61–90.

[11] A. Mielke, *Deriving new evolution equations for microstructures via relaxation of variational incremental problems*, Comp. Meth. Appl. Meth. Eng. **193, No. 48-51** (2004) 5095–5127.

[12] M. Lambrecht, C. Miehe, J. Dettmar, *Energy Relaxation of Non-Convex Incremental Stress Potentials in a Strain-Softening Elastic-Plastic Bar*, Int. J. Solids Struct. **40,Issue 6** (2003) 1369–1391.

[13] M. Ortiz, E.A. Repetto, *Nonconvex energy minimisation and dislocation in ductile single crystals*, J. Mech. Phys. Solids, **47**, 2 (1999) 397–462.

Subspace Correction for Domains with Mutiple Scales

Ralf Kornhuber
(joint work with H. Yserentant)

Multigrid methods and multiscale finite element methods are closely related in the sense that in both cases a suitable resolution and decomposition of scales is cruical for efficiency. In this talk this is illustrated on two examples.

First we consider domains with complicated possibly fractal boundary and explain how coarse grid basis functions can be suitably adapted by truncation, or, equivalently, a suitable modification of restriction.

Then we consider a diffusion problem on a multiscale domain involving a network of fractures with width η. The diffusion k_0 inside the fractures is much larger than in the remaining porous matrix. We strive for robustness for $\eta \to 0$ and $k_0 \to \infty$. To this end, we use anisotropic quadrilaterals for the fracture network and usual isotropic triangles in the porous matrix. For the solution of the resulting discrete problem, we propose a hierachical domain decomposition algorithm seperating fractures from the porous matrix. We prove robust convergence of the associated subspace correction method and illustrate our theoretical results by numerical computations.

Finite temperature coarse-graining of atomistic models: a possible computational approach

Frédéric Legoll
(joint work with Xavier Blanc, Claude Le Bris and Carsten Patz)

In this work, we consider the derivation of reduced models for discrete systems, along with the design of efficient computational approaches, in a constant temperature setting. In short, our aim is to use standard asymptotic tools of probability (such as Large Deviations Principles) to design a computational strategy.

Consider an atomistic system consisting of N particles, at positions $X = \left(X^1, \dots \ \dots, X^N\right) \in \mathbb{R}^{dN}$, where d is the space dimension (d=1, 2 or 3). Provide this system with an energy $V(X) = V\left(X^1, \dots, X^N\right)$ and allow the particles to sample $\mathbb{R}^d$. The finite temperature thermodynamical properties of the material are obtained from canonical ensemble averages,

$$\langle \Phi \rangle = \frac{\displaystyle\int_{\mathbb{R}^{dN}} \Phi(X)\, \exp(-\beta V(X))\, dX}{\displaystyle\int_{\mathbb{R}^{dN}} \exp(-\beta V(X))\, dX}, \tag{1}$$

where Φ is the observable of interest and β is proportional to the inverse temperature. Computing such canonical averages is a standard task of computational materials science. Of course, the major difficulty comes from the N-fold integral,

where N, the number of particles, is extremely large. One possible method is to compute (1) as a long-time average

$$\langle \Phi \rangle = \lim_{T \to +\infty} \frac{1}{T} \int_0^T \Phi(X_t)\, dt \tag{2}$$

along the trajectory generated by the stochastic differential equation

$$dX_t = -\nabla V(X_t)\, dt + \sqrt{2\beta^{-1}}\, dW_t, \tag{3}$$

where W_t is a standard dN-dimensional Brownian motion.

It is often the case that observables of interest do not depend on the positions of *all* the atoms, but only on *some* of them (for instance, because these atoms are located in a region of interest, where some particular phenomenon occurs). We assume that this set of interesting atoms (also called *repatoms*) is given *a priori*, and we denote by X_r their positions. We hence write

$$X = \left(X^1, \ldots, X^N\right) = (X_r, X_c), \quad X_r \in \mathbb{R}^{dN_r}, \quad X_c \in \mathbb{R}^{dN_c}, \quad N = N_r + N_c,$$

and our aim is to compute (1) for such observables, that is

$$\langle \Phi \rangle = Z^{-1} \int_{\mathbb{R}^{dN}} \Phi(X_r)\, \exp(-\beta V(X))\, dX \tag{4}$$

where $Z = \displaystyle\int_{\mathbb{R}^{dN}} \exp(-\beta V(X))\, dX$, by a cheaper method than (2)-(3).

Another question of interest concerns the free energy of the reduced system,

$$A(X_r) = -\frac{1}{\beta} \ln \int_{\mathbb{R}^{dN_c}} \exp(-\beta V(X_r, X_c))\, dX_c.$$

When $N_c \to +\infty$, this energy diverges. The meaningful quantity is the free energy per (removed) particle, $A(X_r)/N_c$. Can this quantity be efficiently computed, in the limit $N_c \to +\infty$?

In [1], we have addressed these question in a one-dimensional setting, using a thermodynamic limit approach (that is, we consider the limit $N_c \to +\infty$). It turns out that actually only the structure of the physical system needs to be one-dimensional: the space in which the atoms vary may be $\mathbb{R}^d$, $d \geq 1$. Our strategy hence applies to chain-like systems, such as polymers. The output of our study is an efficient, and apparently new, computational strategy, whose accuracy is grounded on standard probability theory arguments.

We have considered the case of next-to-nearest-neighbour interactions:

$$V(X) = \sum_{i=1}^{N-1} U_1\left(X^{i+1} - X^i\right) + \sum_{i=1}^{N-2} U_2\left(X^{i+2} - X^i\right).$$

The simpler case of nearest-neighbour interactions corresponds to $U_2 \equiv 0$. In the case of a unique repatom (generalization to the case of several repatoms is easy),

it turns out that the average (4) can be recast as an expectation value:

$$\langle \Phi \rangle = \mathbb{E}\left[\Phi\left(\frac{1}{N}\sum_{i=1}^{N} Y_i\right)\right]$$

for random variables Y_i that are a realization of a Markov chain. Hence, using a Law of Large Numbers argument, we can compute a good approximation of the average (4). In turn, limits of free energies can be handled with classical Large Deviations arguments.

Such an approach may also be considered as a first step toward the numerical analysis of methods commonly used in practice [2], and the assessment of the simplifying assumptions upon which they rely.

References

[1] X. Blanc, C. Le Bris, F. Legoll, C. Patz, *Finite-temperature coarse-graining of one-dimensional models: mathematical analysis and computational approaches*, INRIA preprint RR-6544 (may 2008), available at `http://hal.inria.fr/inria-00282107/en/`.

[2] L. M. Dupuy, E. B. Tadmor, R. E. Miller, R. Phillips, *Finite temperature Quasicontinuum: Molecular dynamics without all the atoms*, Phys. Rev. Lett. **95** (2005), 060202.

Analysis of Quasicontinuum Approximation: Statics and Dynamics

Ping Lin

We consider that materials are modeled by a large number of atomic particles where any one of particles interacts with all others. Directly solving the whole system (the lattice statics) provides a powerful and accurate tool of analysis in the lattice scale. However, because the number of atomic particles in a material is huge, it is often impossible to directly solve the whole system to obtain the material properties. The problem is often simplified by only considering the interaction of one particle with its nearby particles (or even its nearest neighbors). People believe that the simplified problem is a good approximation to the original full-interaction problem. But there is no rigorous analysis available. In the 1D case we provide an estimation of the error between the solution of simplified problem and the solution of the full-interaction problem for the typical Lennard-Jones pair interaction potential. The argument applies to other similar pair interaction potentials as well. From the estimation we can conclude that such simplification is often good enough for short-range pair interaction potentials.

On the other hand, even for the simplified problem the system is still huge and impossible to be solved directly. Fortunately in many practical problems defects only occur in some local, perhaps small, regions. We need to consider the lattice scale in these small defect regions. This helps with the design of approximation methods for the simplified problem. Recently quasi-continuum approximation (See [7, 6]) gains noticeable attention in engineering literatures. The key idea is that in the region (called local approximation region) where no defects occur we can

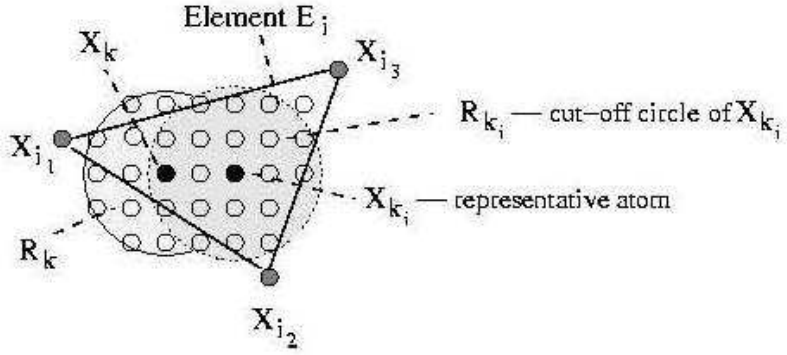

FIGURE 1. A triangular element in QC

consider it at the macro-scale and the theory of continuum material elasticity may apply. The QC approximation solves a fully atomistic problem in regions where the material contains defects and/or has large deformation gradients, but uses continuum finite elements to effectively integrate out the majority of the atomistic degrees of freedom in regions of the material where deformation gradients are small.

The QC approximation is incorporated with a computational technique called nonconforming finite element method. The domain that the material occupied may be triangulated first. The atomic particles are assumed to deform uniformly in each triangular element which corresponds to using a piecewise linear function to approximate the solution in the usual finite element method. We assign a representative particle in each element. The idea of the quasi-continuum method is based on the following approximation: the potential energy associated with any particle in the triangular element is approximately equal to the potential energy associated with the representative atom (See Figure 1). Note that the exact solution in a standard finite element error estimate is a solution of continuum partial differential equations. Here the exact solution is of discrete equations which are not close to any conventional partial differential equations (See [1, 3]. As an illustrative example, we consider the system of Figure 1. The total energy reads:

$$E(z) = \frac{1}{2}\sum_{i=1}^{N}\sum_{k=1}^{m_i}\sum_{\ell\in R_k,\ell\neq k}\phi(|z_k - z_\ell|) + \sum_{i=1}^{N}\sum_{k=1}^{m_i}E_f(z_k), \tag{1}$$

where E_f is an energy corresponding to an external force, the letter i is specially assigned to the index for the i-th triangular element E_i, k is the index for atoms in the element E_i, atom k_i is the representative atom of E_i, m_i is the number of atoms in E_i, and N is the number of triangular elements. $|\cdot|$ represents the Euclidean length of a vector. The stable configuration (i.e. the "correct" solution) of the material is identified with the minimizer $\hat{z}$ of the potential energy $E(z)$:

$$E(\hat{z}) = \min_{z} E(z). \tag{2}$$

We assume that in each triangle E_i the atoms are deformed uniformly (piecewise linear basis functions) and then the QC approximate potential energy reads

$$E_{qc}(Z^h) = \frac{1}{2}\sum_{i=1}^{N} m_i \sum_{\ell \in R_{k_i}} \phi(|Z_\ell - Z_{k_i}|) + \sum_{i=1}^{N}\sum_{k=1}^{m_i} E_f(Z_k), \tag{3}$$

where Z^h is a vector collecting all positions of atoms at the vertices of triangle elements, and Z_ℓ and Z_{k_i} are positions of atoms interpolated through positions of atoms at triangular vertices of Z^h. We would like to estimate the error between the "correct" solution $\hat{z}$ and the QC solution $\hat{Z}^h$. We recently present a framework of analysis and for a 2D case we obtain that the discrete error of the QC without defects is less than $C\left(h + \sqrt{\sum_{i=1}^{N} \frac{b_i^2}{m_i}/M}\right)$ under a few assumptions. Here h is the element size, $M = \sum_{i=1}^{N} m_i$ is the total number of atoms, m_i is the number of atoms in the triangular element E_i and b_i is the number of atoms near at least one boundary of E_i and is less than a constant times the number of atoms located at the longest side of E_i. The analysis may also be applied to the case with defects in a relatively small region. In that case we expect that the discrete error of the QC is less than $C\left(h + \sqrt{\sum_{i\in I_{nd}} \frac{b_i^2}{m_i}/M} + \sqrt{M_d/M}\right)$, where I_{nd} collects all elements which are not involved with any defects and M_d stands for the number of atoms in those elements involved with defects.

An important direction in multiscale research is the development of algorithms that allow for dynamic effects to be modeled in an atomistic/continuum framework without losing the essential philosophy i.e. the systematic removal of a large fraction of the degrees of freedom and the explicit treatment of only a small subset of the atoms in the problem. The quasi-continuum and finite element idea may be applied to approximate material dynamics. This gives a coarse-grained dynamical model. We realize that the difference between the solutions of the coarse-grained model and the atomistic model will not generally be small since their frequency and phase of oscillation are quite different. Then an interesting problem is this: in what sense may the dynamic QC be good? From the above observation we expect that the method may possibly be good if there is no oscillatory effect (for example, in the sense of time average or small damping). We recently relate the analysis to the theory of conservation laws (p-system) at least for cases with nearest neighbor interactions (See [2, 5, 4]). The p-system may be of mixed type due to the nonconvex potential energy. There is no existence and uniqueness theory available in general. However, it is possible to construct the solution of a Riemann problem with given admissible conditions (relevant to the small damping term introduced). We recently sketch an outline of such analysis and present numerical studies for a very basic nearest neighbour interacting model. We find that the dynamical solution is the limit of the solution of the damped system if the distance of any neighboring pair of atoms locates in the convex region of the Lennard-Jones

potential. Convergence analysis techniques for numerical conservation laws are fundamental in error analysis of the coarse-grained dynamical model.

References

[1] P. Lin, Theoretical and numerical analysis for the quasi-continuum approximation of a material particle model, Mathematics of Computation 72 (2003), 657-675.
[2] P. Lin , A nonlinear wave equation of mixed type for fracture dynamics, Preprint.
[3] P Lin, Convergence analysis of a quasi-continuum approximation for a two-dimensional material, SIAM J Numer Anal 45 (2007), No.1, 313-332
[4] P Lin and P Plechac, Numerical studies of a coarse-grained approximation for dynamics of an atomic chain, International Journal for Multiscale Computational Engineering 5 (2007), 351-367.
[5] P. Lin and C.W. Shu, Numerical solution of a virtual internal bond model for material fracture, Physica D: Nonlinear Phenomena 167 (2002), No 1-2, 101-121.
[6] R. Miller, E.B. Tadmor, The quasicontinuum method: Overview, applications and current directions, *J of Computer-Aided Material Design* 9 (2002), 203-239.
[7] E.B. Tadmor, M. Ortiz and R. Phillips, Quasicontinuum analysis of defects in solids, Philosophical Magazine A 73 (1996), 1529-1563.

Sharp Stability Estimates for Quasicontinuum Methods: Accuracy Near Instabilities

Mitchell Luskin
(joint work with Matthew Dobson, Christoph Ortner)

The formation and motion of lattice defects such as cracks, dislocations, or grain boundaries, occurs when the lattice configuration loses stability, that is, when an eigenvalue of the Hessian of the lattice energy functional becomes negative. When the atomistic energy is approximated by a hybrid energy that couples atomistic and continuum models, the accuracy of the approximation can only be guaranteed near deformations where both the atomistic energy as well as the hybrid energy are stable. We propose, therefore, that it is essential for the evaluation of the predictive capability of atomistic-to-continuum coupling methods near instabilities that a theoretical analysis be performed, at least for some representative model problems, that determines whether the hybrid energies remain stable *up to the onset of instability of the atomistic energy.*

We formulate a one-dimensional model problem with nearest and next-nearest neighbor interactions and use rigorous analysis, asymptotic methods, and numerical experiments to obtain such sharp stability estimates for the basic conservative quasicontinuum (QC) approximations. Our results show that the consistent quasi-nonlocal QC approximation correctly reproduces the stability of the atomistic system, whereas the inconsistent energy-based QC approximation incorrectly predicts instability at a significantly reduced applied load that we describe by an analytic criterion in terms of the derivatives of the atomistic potential.

Numerical experiments show that the spectrum of a linearized QCF operator is identical to the spectrum of a linearized energy-based quasi-nonlocal quasicontinuum operator (QNL), which we know from our previous analyses to be positive

below the critical load. However, the QCF operator is non-normal and it turns out that it is not generally positive definite, even when all of its eigenvalues are positive. Using a combination of rigorous analysis and numerical experiments, we investigate in detail for which choices of "function spaces" the QCF operator is stable, uniformly in the size of the atomistic system.

Force-based multi-physics coupling methods are popular techniques to circumvent the difficulties faced in formulating consistent energy-based coupling approaches. Even though the QCF method is possibly the simplest coupling method of this kind, we anticipate that many of our observations apply more generally.

References

[1] Dobson, M., Luskin, M.: Analysis of a force-based quasicontinuum approximation. Mathematical Modelling and Numerical Analysis **42**, 113–139 (2008)
[2] Dobson, M., Luskin, M.: An analysis of the effect of ghost force oscillation on the quasicontinuum error. Mathematical Modelling and Numerical Analysis **43**, 591–604 (2009)
[3] Dobson, M., Luskin, M.: An optimal order error analysis of the one-dimensional quasicontinuum approximation. SIAM. J. Numer. Anal. **47**, 2455–2475 (2009)
[4] M. Dobson, M. Luskin, and C. Ortner. Stability, instability, and error of the force-based quasicontinuum approximation. arXiv:0903.0610, 2009.
[5] Dobson, M., Luskin, M., Ortner, C.: Accuracy of quasicontinuum approximations near instabilities (2009). ArXiv:0905.2914v2
[6] Dobson, M., Luskin, M., Ortner, C.: Sharp stability estimates for the force-based quasicontinuum method (2009). ArXiv:0907.3861
[7] Ortner, C., Süli, E.: Analysis of a quasicontinuum method in one dimension. Mathematical Modelling and Numerical Analysis **42**, 57–91 (2008)

Adaptive variational multiscale methods

Axel Malqvist

1. Introduction

The adaptive variational multiscale [2, 3, 4] (AVMS) method is a novel multiscale method that builds on the combination of:

- The variational multiscale framework [1].
- A systematic technique for numerical approximation of the fine scale part of the solution based on solving localized subgrid problems on patches.
- A posteriori error estimates and adaptive algorithms that provide control of numerical error as well as automatic tuning of critical discretization parameters.

In this abstract we give a condensed presentation of the AVMS method and the energy norm a posteriori error estimates for an elliptic model problem with multiscale features in the conductivity, see [3] for further details and numerical examples. A mixed version of the method is presented in [2] and convection dominated problems are considered in [4].

2. The variational multiscale method

We shall study the following model problem: find u such that

$$-\nabla \cdot a\nabla u = f \text{ in } \Omega, \quad u = 0 \text{ on } \Gamma, \tag{1}$$

where Ω is a polygonal domain in $\mathbf{R}^d$, $d = 1, 2$, or 3 with boundary Γ, $f \in L^2(\Omega)$, and $a \in L^\infty(\Omega)$ satisfies $a(x) \geq a_0 > 0$ for all $x \in \Omega$ has multiscale features.

The variational form of (1) reads: find $u \in \mathcal{V} = H_0^1(\Omega)$ such that

$$a(u, v) = (f, v) \quad \text{for all } v \in \mathcal{V}, \tag{2}$$

with the bilinear form $a(u, v) = (a\nabla u, \nabla v)$, for all $u, v \in \mathcal{V}$.

The Variational Multiscale method [1] (VMS) is an important framework for constructing multiscale methods. The idea is to decompose the solution into fine $u_f \in \mathcal{V}_f$ and coarse $u_c \in \mathcal{V}_c$ scale contributions as follows

$$\begin{aligned} a(u_c, v_c) + a(u_f, v_c) &= (f, v_c) \quad \text{for all } v_c \in \mathcal{V}_c, \\ a(u_f, v_f) = (f, v_f) - a(u_c, v_f) &=: (R(u_c), v_f) \quad \text{for all } v_f \in \mathcal{V}_f. \end{aligned} \tag{3}$$

The fine scale equation are solved in terms of the coarse scale residual $R(u_c)$, and finally eliminate the fine scale solution from the coarse scale equation. This procedure leads to the modified coarse scale equation (4) where the modification accounts for the effect of fine scale behavior on the coarse scales.

$$a(u_c, v_c) + a(\mathcal{T}R(u_c), v_c) = (f, v_c) \quad \text{for all } v_c \in \mathcal{V}_c. \tag{4}$$

Here $\mathcal{T}$ represents an approximate solution operator of the fine scale problem. In several works various ways of analytical modeling of $\mathcal{T}$ are investigated [1].

3. Approximation of fine scales

In the AVMS [2, 3, 4] the fine scale equations in (3) are decoupled and solved numerically on patches. The idea is to decouple the fine scale equations by including a partition of unity in the right hand side of the fine scale part of equation (3) and then to solve the resulting problems on patches.

We introduce a partition $\mathcal{K} = \{K\}$ of the domain Ω into coarse shape regular elements K of diameter H and we let $\mathcal{N}$ be the set of coarse nodes and let $\mathcal{V}_c$ be the space of continuous piecewise polynomials of degree one defined on $\mathcal{K}$. Let $u_f = \sum_{i \in \mathcal{N}} u_{f,i}$ where

$$a(u_{f,i}, v_f) = (\varphi_i R(u_c), v_f) \quad \text{for all } v_f \in \mathcal{V}_f, \tag{5}$$

and $\{\varphi_i\}_{i \in \mathcal{N}}$ is a partition of unity e.g. the set of Lagrange basis functions in $\mathcal{V}_c$, be the solution to the decoupled fine scale equations.

We introduce this expansion of u_f in the right hand side of the fine scale equation (3) and get: find $u_c \in \mathcal{V}_c$ and $u_f = \sum_{i \in \mathcal{N}} u_{f,i} \in \mathcal{V}_f$ such that

$$\begin{aligned} a(u_c, v_c) + a(u_f, v_c) &= (f, v_c) \quad \text{for all } v_c \in \mathcal{V}_c, \\ a(u_{f,i}, v_f) &= (\varphi_i R(u_c), v_f) \quad \text{for all } v_f \in \mathcal{V}_f \text{ and } i \in \mathcal{N}. \end{aligned} \tag{6}$$

The next step is to solve the fine scale equations approximately. For each element in the partition of unity we associate a domain ω_i on which we solve Dirichlet

problems. The local domain ω_i contains the support of the element in the partition of unity and is large enough to give a good approximate solution. The quality of the solution is controlled by error estimates. We now define the local finite element space $\mathcal{V}_f^h(\omega_i)$ associated with node i. We refine the coarse mesh on the patch ω_i and let $\mathcal{V}_f^h(\omega_i)$ be the fine part of the hierarchical basis on this mesh.

The resulting method reads: find $U_c \in \mathcal{V}_c$ and $U_f = \sum_{i\in\mathcal{N}} U_{f,i}$ where $U_{f,i} \in \mathcal{V}_f^h(\omega_i)$ such that

$$\begin{aligned} a(U_c, v_c) + a(U_f, v_c) &= (f, v_c) \quad \text{for all } v_c \in \mathcal{V}_c, \\ a(U_{f,i}, v_f) &= (\varphi_i R(U_c), v_f) \quad \text{for all } v_f \in \mathcal{V}_f^h(\omega_i) \text{ and } i \in \mathcal{N}. \end{aligned} \tag{7}$$

If we just have fine scale features on part of the domain we only solve local problems for these areas. We denote coarse nodes in these areas $\mathcal{F}$ and the rest $\mathcal{C}$. If we write the method in matrix form we would get,

$$(A + T)U_c = b - d, \tag{8}$$

where A and b are the standard finite element stiffness matrix and load vector and the T matrix and d vector arises in analogy with equation (4) since $\mathcal{T}(R(U_c))$ is affine in U_c.

4. A posteriori error estimates

In [2] we present the following a posteriori error estimate for the adaptive variational multiscale method in the energy norm $\|e\|_a^2 = a(e, e)$.

Theorem 4.1. *It holds,*

$$\begin{aligned} \|e\|_a^2 \leq C \sum_{i\in\mathcal{C}} \|H\mathcal{R}(U_c)\|_{\omega_i}^2 \|\frac{1}{\sqrt{a}}\|_{L^\infty(\omega_i)}^2 \\ + C \sum_{i\in\mathcal{F}} \left(\|\sqrt{H}\Sigma(U_{f,i})\|_{\partial\omega_i\setminus\Gamma}^2 + \|h\mathcal{R}_i(U_{f,i})\|_{\omega_i}^2 \right) \|\frac{1}{\sqrt{a}}\|_{L^\infty(\omega_i)}^2, \end{aligned} \tag{9}$$

where

$$(-\Sigma(U_{f,i}), v_f)_{\partial\omega_i} = (\varphi_i R(U_c), v_f)_{\omega_i} - a(U_{f,i}, v_f)_{\omega_i}, \quad \textit{for all } v_f \in V_f^h(\bar{\omega_i}). \tag{10}$$

Here $\mathcal{R}(U_c)$ and $\mathcal{R}_i(U_{f,i})$ are bounds of the coarse and fine scale residual, $\Sigma(U_{f,i})$ is a variational approximation [1] of the normal flux $\partial_n U_{f,i}$ in $L^2(\partial\omega_i)$, and $\mathcal{V}_f^h(\bar{\omega_i})$ is the space of piecewise linear continuous functions defined on a subgrid partition of ω_i that are not required to be zero on the boundary $\partial\omega_i$ of ω_i. We can easily understand the contributions to the error. If no fine scale equations are solved we obtain the first term in the estimate; the first part of the second sum measures the effect of restriction to patches; and finally the second part measures the influence of the fine scale mesh parameter h. Using these indicators one may construct an adaptive algorithm for automatic tuning of the size of the patches and the subgrid resolution, see [3] for details.

References

[1] T. J. R. Hughes, G. R. Feijóo, L. Mazzei and J.-B. Quincy, *The variational multiscale method - a paradigm for computational mechanics*, Comput. Methods Appl. Mech. Engrg. **166** (1998), 3–24.

[2] M. G. Larson and A. Målqvist, *A mixed adaptive variational method with application in oil reservoir simulation*, to appear in Math. Models Methods Appl. Sci.

[3] M. G. Larson and A. Målqvist, *Adaptive variational multiscale methods based on a posteriori error estimates: energy norm estimates for elliptic problems*, Comput. Methods Appl. Mech. Engrg., **196** (2007), 2313–2324.

[4] M. G. Larson and A. Målqvist, *An adaptive variational multiscale method for convection-diffusion problems*, Comm. Numer. Methods Engrg., **25** (2009), 65–79.

A New Multigrid Method for Molecular Mechanics Model

Pingbing Ming

(joint work with J.R. Chen and W. E)

The total energy of the atomistic model of the crystalline solids can be written as

$$E^{\mathrm{tot}}(\boldsymbol{y}) = V(\boldsymbol{y}_1, \ldots, \boldsymbol{y}_N) - \sum_{i=1}^{N} \boldsymbol{f}_i \cdot \boldsymbol{y}_i,$$

where $\boldsymbol{y}_i$ and $\boldsymbol{x}_i$ are the positions of the i-th atom in the deformed and undeformed configurations, respectively, and $-\boldsymbol{f}_i \cdot \boldsymbol{y}_i$ is the work done by the external force $\boldsymbol{f}_i$ on the i-th atom, The energy V often takes the form:

$$V(\boldsymbol{y}) = \sum_{i,j} V_2(\boldsymbol{y}_i/\epsilon, \boldsymbol{y}_j/\epsilon) + \sum_{i,j,k} V_3(\boldsymbol{y}_i/\epsilon, \boldsymbol{y}_j/\epsilon, \boldsymbol{y}_k/\epsilon) + \cdots,$$

where ϵ is the lattice constant, and V_2 is a two-body potential while V_3 is a three-body potential.

The atomic configuration is given by solving the following minimization problem:

$$\boldsymbol{y} = \operatorname{argmin} E^{\mathrm{tot}}(\boldsymbol{y}). \tag{1}$$

The crystal is in equilibrium with applied force $\boldsymbol{f}$ if for any i,

$$-\frac{\partial V}{\partial \boldsymbol{y}_i} + \boldsymbol{f}_i = \boldsymbol{0}.$$

Applying the traditional iteration methods to the above minimization problem, nine out of ten, we either obtain the relevant configurations with high cost or we get the incorrect configurations. This is mainly due to the fact that the total energy is nonconvex with respect to the atom positions, which is a natural consequence of the symmetry of the underlying lattice and the translation invariance of the potential function [6]. By [4, 5], the elastically deformed state we are looking for is only a local minimizer instead of a global minimizer. Therefore, once we start with a *bad* initial guess, the traditional iteration procedure may lead to either meaningless local minimizer, or *jumps into* a local minimizer basin that is far away from the relevant configuration. Find a good initial guess is of ultra importance to solve (1).

We have proved in [4, 5] that, under certain stability conditions, around the solution of the Cauchy-Born elasticity model, there is a local minimizer of the atomistic model nearby. Motivated by this result, we solve (1) with the solution of the Cauchy-Born elasticity model as an initial guess.

The Cauchy-Born elasticity model of the crystalline solids can be described as follows. Let Ω be the domain occupied by the material in the undeformed state. The displacement field $\boldsymbol{u}$ is determined by the following minimization problem:

$$\boldsymbol{u} = \operatorname*{argmin}_{\boldsymbol{v}\in X} I(\boldsymbol{v}),$$

where

$$I(\boldsymbol{v}) = \int_\Omega \big(W\big(\nabla \boldsymbol{v}(\boldsymbol{x})\big) - \boldsymbol{f}(\boldsymbol{x})\cdot \boldsymbol{v}(\boldsymbol{x})\big)\,\mathrm{d}\boldsymbol{x}, \tag{2}$$

where W is obtained from Cauchy-Born rule [1], we refer to [4] for examples of such stored energy functional W.

Our algorithm can be described as follows:

Step 1: Initialization: solve Cauchy-Born elasticity problem (2) on the 0-th level with trivial initial guess to obtain $\tilde{\boldsymbol{u}}_0$.

Step 2: For $i = 1, \ldots, l$,

(1) Interpolate

$$\boldsymbol{u}_i = I_{i-1}^i \tilde{\boldsymbol{u}}_{i-1},$$

where I_{i-1}^i is the standard finite element interpolation operator.

(2) Solve Cauchy-Born elasticity (2) on the i-th level with initial guess $\boldsymbol{u}_i$ to obtain $\tilde{\boldsymbol{u}}_i$.

(3) Define the Cauchy-Born state as

$$\boldsymbol{y}_{\mathrm{CB}} = \boldsymbol{x} + \tilde{\boldsymbol{u}}_i(\boldsymbol{x}).$$

Step 3: Relaxation: solve MM (1) with the Cauchy-Born state $\boldsymbol{y}_{\mathrm{CB}}$ as the initial guess.

We demonstrate the efficiency of this algorithm by test tension in [111] direction for aluminum (Al). The atoms are interacted with the embedded-atom method (EAM) potential [3]. We impose the Dirichlet boundary condition on [111] direction (principal direction), and impose the periodic boundary conditions on both $[11\bar{2}]$ and $[\bar{1}10]$ directions. The hexahedron element with the standard eight-point Gauss numerical integration scheme is employed to discretize the Cauchy-Born elasticity problem. We report the stress-strain cure and the log-log plot of CPU time vs. system size in Figure 1.

In the stress strain curve, at "." , linear scaling is preserved; while at "∇" , linear scaling is lost. The elasticity instability firstly occurs at point "C" since the macroscopic stability condition [4] does not hold after this critical point. Results after "C" are unreliable. The critical strain is about 0.08. By Figure 1, we conclude that our method is linear scaling. We refer to [2] for other examples that includes test problems with inhomogeneous deformation.

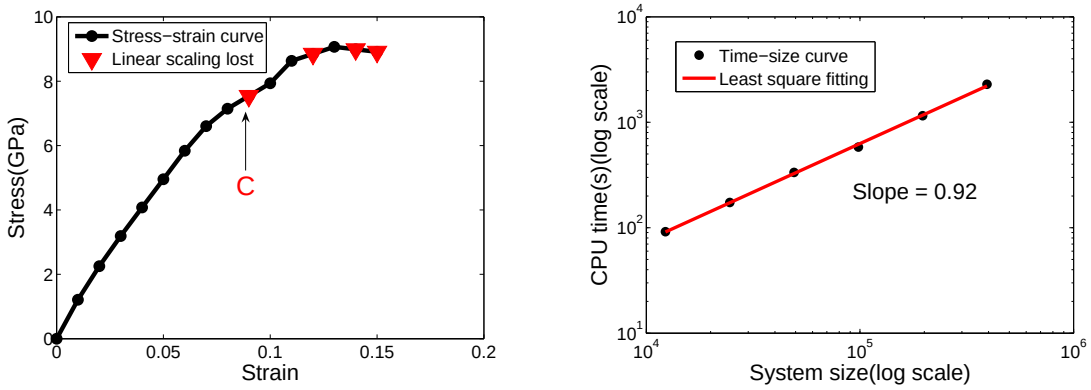

FIGURE 1. Left: Stress-strain curve of Al under tension; Right: CPU time(Log-log plot).

REFERENCES

[1] M. Born and K. Huang, *Dynamical Theory of Crystal Lattices*, Oxford University Press, 1954.
[2] J.R. Chen, P.B. Ming and W. E, *An efficient multigrid method for molecular mechanics models*, preprint, 2009.
[3] M.S. Daw and M.I. Baskes, *Embedded-atom-method: derivation and application to impurities, surfaces and other defects in metals*, Phys. Rev. B **29**(1984), 6443–6453.
[4] W. E and P.B. Ming, *Cauchy-Born rule and the stability of the crystalline solids: static problems*, Arch. Rational Mech. Anal. **183**(2007), 241–297.
[5] W. E and P.B. Ming, *Cauchy-Born rule and the stability of the crystalline solids: dynamic problems*, Acta Math. Appl. Sin. Engl. Ser. **23**(2007), 529–550.
[6] G. Friesecke and F. Theil, *Validity and Failure of the Cauchy-Born hypothesis in a two-dimensional mass-spring lattice*, J. Nonlinear. Sci. **12**(2002), 445–478.

Locally conservative multiscale methods for Darcy equations

EUN-JAE PARK

This presentation consists of two parts. The first part is based on joint work with M. Wheeler. We study multiscale mortar mixed finite element discretizations for model elliptic problems introduced by Arbogast *et al.* [1]. This approach is based on domain decomposition theory and mortar finite elements [2]. In this method, flux continuity is imposed via a mortar finite element space on a coarse grid scale, while the equations in the coarse elements (or subdomains) are discretized on a fine grid scale.

We consider an interface problem involving only the mortar pressure which arises from the mortar mixed formulation. The interface formulation is useful in deriving a bound on the error in the mortar space. Moreover, it is the basis for implementation of parallel domain decomposition methods. However, in the previous work, the mortar pressure error was measured in a semi-norm arising from the interface formulation. It applies to the case where the model problem is symmetric positive definite. It should be noted that in many interesting applications, it is

important to be able to treat more general problems including nonsymmetric tensor coefficients and/or convection-diffusion equations. Moreover, in the nonlinear case, the use of the superposition principle is not applicable for the error analysis. Therefore, we introduce a new approach for treating interface problem and prove various stability estimates based on inf-sup conditions related to the mortar pressure variable. Optimal fine scale convergence is obtained by an appropriate choice of mortar grid and polynomial space of approximation.

Finally, we discuss recent results treating convection-diffusion equations using this new approach. We extend the method to treat slightly compressible Darcy flows in porous media. Parallel numerical simulations on some multiscale benchmark problems are given to show the efficiency and effectiveness of the method [3].

In the second part of the presentation, we introduce so called cell boundary element (CBE) methods. This part is joint work with Youngmok Jeon. The CBE method is designed in such a way that they enjoy the mass conservation at the element level and the normal component of fluxes at inter-element boundaries are continuous for unstructured triangular meshes. The MsCBE method is based on recently introduced nonconforming cell boundary element (CBE) methods [7, 6].

Now we introduce a flux preserving elliptic multiscale problem solver (MsCBE). The multiscale cell boundary element method is a natural extension of the CBE method to multiscale problems: find $v_{h,\epsilon} \in V_h$ such that

$$\int_{e_p} [(a_\epsilon \nabla v_{h,\epsilon} \cdot \nu)]\, ds = -\int_{e_p} [(a_\epsilon \nabla G) \cdot \nu]\, ds, \tag{1}$$

where the bubble function G satisfies

$$-\nabla \cdot (a_\epsilon(\mathbf{x})\ \nabla G) = f \quad \text{on } T \tag{2}$$

with the boundary condition $G = 0$ on ∂T. The finite dimensional multiscale function space V_h is spanned by functions, which satisfy the homogeneous equation locally, that is,

$$-\nabla \cdot (a_\epsilon(\mathbf{x})\ \nabla \phi_{h,\epsilon}) = 0 \quad \text{on } T \tag{3}$$

with properly given boundary conditions. We use an oversampling technique to obtain the local basis (in (3)) as in [8]. Then the MsCBE method yields solution and its flux conserving flux formula as follows:

$$u_{h,\epsilon} = v_{h,\epsilon} + G \quad \text{and} \quad a_\epsilon \nabla u_{h,\epsilon} = a_\epsilon \nabla v_{h,\epsilon} + a_\epsilon \nabla G. \tag{4}$$

The detailed description and convergence of the CBE and MsCBE methods can be found in [7, 5].

For comparison purpose, we consider an approximate solution by the multiscale finite element method (MsFEM, [8]): find $u^{ms}_{h,\epsilon} \in V_h$ such that

$$\int_\Omega a_\epsilon \nabla u^{ms}_{h,\epsilon} \cdot \nabla r_h dx = \int_\Omega f r_h dx, \quad r_h \in V_h. \tag{5}$$

For the MsFEM, the flux-preserving flux recovery formula is not available to the best of our knowledge. The MsFEM and MsCBE are composed of two processes to obtain solutions:

- construction of the local basis and bubble function in (3) and (2) (the fine scale solver)
- the coarse scale FEM or CBE solver ((5), (1)).

It has been observed that fine scale solver as well as coarse grid solver should be locally mass conservative in order to have flux conservation at the element level. Moreover, our method is free from the resonance with the mesh size h and ϵ.

References

[1] T. Arbogast, G. Pencheva, M. F. Wheeler, and I. Yotov, A multiscale mortar mixed finite element method. Multiscale Model. Simul. Vol. **6**, No. 1, (2007), pp. 319–346.

[2] C. Bernardi, Y. Maday, and A. T. Patera, *A new nonconforming approach to domain decomposition: The mortar element method*, in Nonlinear partial differential equations and their applications, H. Brezis and J. L. Lions, eds., Longman Scientific & Technical, UK, 1994.

[3] M.-Y. Kim, E.-J. Park, S. G. Thomas, and M. F. Wheeler, A multiscale mortar mixed finite element method for slightly compressible flows in porous media, *J. Korean Math. Soc.* **44** (2007), No. 5, pp. 1103-1119

[4] E.-J. Park and M. F. Wheeler, An analysis of multiscal mixed finite element methods, *Preprint*

[5] Y. Jeon, A multiscale cell boundary element method for elliptic problems, Appl. Numer. Math, in press, doi:10.1016/j.apnum.2008.12.029.

[6] Y. Jeon and E.-J. Park, Cell boundary element methods for elliptic problems, Hokkaido Math. J. **36** (2007), no. 4, 669-685.

[7] Y. Jeon and E.-J. Park, *Nonconforming cell boundary element methods for elliptic problems on triangular mesh*, Appl. Numer. Math. **58** (2008), 800-814.

[8] T. Y. Hou and X. H. Wu, A multiscale finite element method for elliptic problems in composite materials and porous media, J. Comput. Phys., **134** (1997), 169-189.

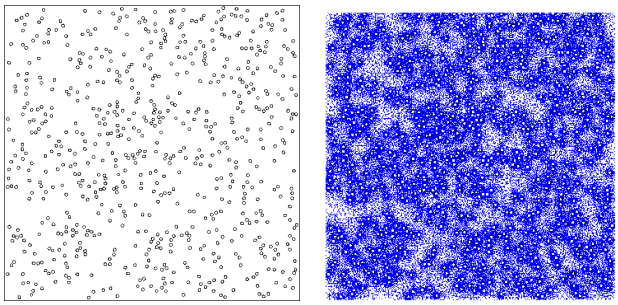

Figure 1. Model domain containing 700 circular inclusions (left) and high quality triangular mesh with more than 110000 nodes (right).

Finite Element Analysis of Particle Reinforced Composites

Daniel Peterseim

Composite materials appear in many practical applications such as the approximation of effective properties of fiber materials, thermal management in electronics industry, and optimal design of electric capacitors; to mention only a few. All these problems have two characteristic features in common: Random microstructures on multiple scales and high contrast in physical properties. These properties are already present in the simple 2-dimensional model of a high contrast composite occupying the domain $Q^* := [-L_1, L_1] \times [-L_2, L_2]$. The (perfectly conducting) inclusions (filler), denoted by $B_i \subset Q^*$, $i = 1, \dots, N$, are assumed to be closed circles of radius r_i not intersecting each other. The so-called matrix (the perforated domain) is denoted by $Q := Q^* \setminus \bigcup_{i=1}^N B_i$. Let $Q^\pm := \{\mathbf{x} \mid x_2 = \pm L_2\}$ be the upper/lower boundary of Q and $Q^{\text{lat}} := \partial Q^* \setminus (\partial Q^+ \cup \partial Q^-)$ be the lateral boundary. We are interested in computing the effective conductivity

$$\hat{a} := \min_{v \in V} I[v] := \frac{1}{2|Q^*|} \int_Q |\nabla v|^2 d\mathbf{x}, \tag{1}$$

of the composite, where the space of admissible functions is given by

$$V := \{v \in H^1(Q) \mid \exists \mathbf{t} \in I\!R^N : v(\mathbf{x}) = t_i \text{ on } \partial B_i,\ v(\mathbf{x}) = \pm 1 \text{ on } \partial Q^\pm\}. \tag{2}$$

A minimizer $u \in V$ of (1) fulfills the corresponding Euler-Lagrange equations:

$$\begin{aligned} \Delta \mathbf{u} = 0,\ \text{in } Q, \quad \mathbf{u}(\mathbf{x}) = \pm 1,\ \text{on } \partial Q^\pm, \quad \tfrac{\partial \mathbf{u}}{\partial \boldsymbol{\nu}} = 0,\ \text{on } Q^{\text{lat}} \\ \mathbf{u}(\mathbf{x}) = t_i,\ \text{on } \partial B_i, \quad \textstyle\int_{\partial B_i} \frac{\partial \mathbf{u}}{\partial \boldsymbol{\nu}} = 0, \quad i = 1, \dots, N. \end{aligned} \tag{3}$$

This model has been introduced in [2] and further been investigated in [3, 1]. Here, it will serve as a reference example for describing the mathematical challenges related to composite materials as well as the newly proposed prototype of solution method.

The main difficulty for a numerical approximation of problem (3) lies in the complexity of the underlying geometry, i.e. the perforated domain Q. Standard finite element methods will suffer from the fact that the computation of suitable

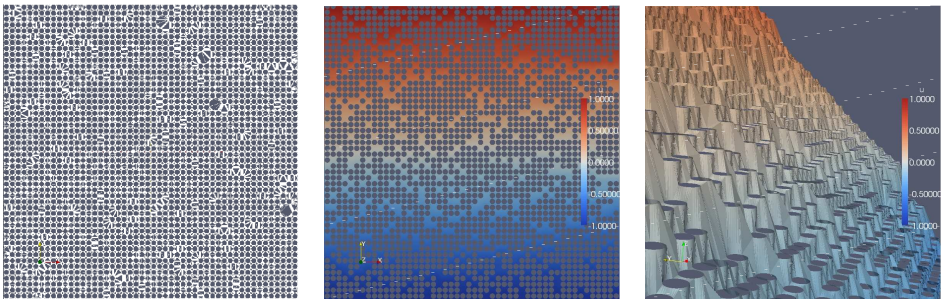

Figure 2. A generalized Delaunay mesh (left) and the corresponding generalized finite element approximation indicated by colors (middle, right).

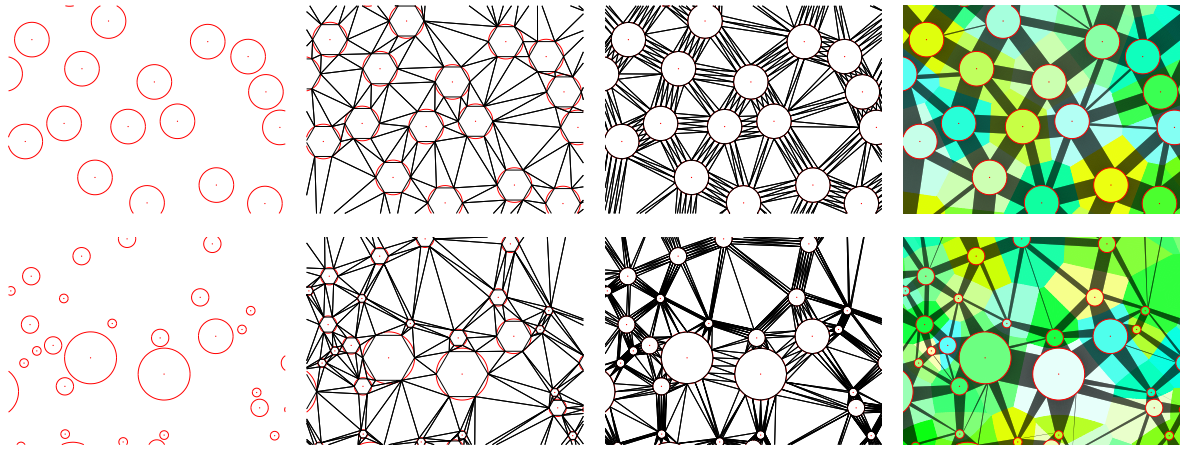

FIGURE 3. Construction of the generalized Delaunay mesh (from left to right): Part of domain Q (equally/non-equally sized inclusions above/below), approximation of Q by regular 6-gons and related Delaunay partition, approximation of Q by regular 20-gons and related Delaunay partition, generalized Delaunay partition and (generalized) Voronoi tessellation of the inclusions.

meshes is expensive, since every hole needs to be resolved by the triangulation in order to derive satisfactory results from standard finite element approximations; Figure 1 illustrates the problem for a model situation. This resolution condition forces even the coarsest available meshes to be very fine, i.e. it forces the minimal mesh size to be of order of the inclusion radii. Due to the shape regularity requirement the minimal number of nodes in the triangulation will further depend critically on the distribution of the inclusions and their distances. This is particularly disadvantageous since problem (3), typically, needs to be solved very often as a part of a statistical investigation of the material properties.

As a first step towards a new class of finite element models, in [4], we are currently developing a generalization of triangular meshes which allow to model the inclusions as weighted vertices. This approach is inspired by the work of Berlyand [2, 3, 1]. A typical generalized mesh $\mathcal{G}$ for equally sized inclusion is depicted in Figure 2. It is based on the Voronoi tessellation of the inclusions defining a neighborhood relation between the inclusions. $\mathcal{G}$ is a subdivision of Q^* into generalized vertices (circles), generalized edges (channels) and triangles. The subdivision reflects physics in the sense that the potential is mainly determined by fluxes between neighboring inclusions, whereas fluxes between inclusions of a certain distance can be neglected (cf. [3]). Such a subdivision can be derived by employing a convergent sequence of polygonal approximations to Q and its corresponding Delaunay triangulations with respect to the corners as it is illustrated in Figure 3.

Based on these new type of meshes a generalized nodal basis defining a generalized conforming Courant finite element space is introduced. A representative shape function is depicted in Figure 2 which shows the related Galerkin approximation to problem (3) for the composite from Figure 2. These shape functions,

similar the classical P1 finite element shape functions, are uniquely defined by their values at the vertices and to some extend linearly interpolated in between.

The new approach is optimal in the sense that the number of unknowns in the discrete problem (and the computational complexity) equals the number of unknowns t_i of the continuous problem (3). Note that additional (0-weighted) vertices can be introduced in the matrix Q to improve the approximation quality whereever necessary. Under additional mild assumptions on the hole distribution the classical a priori error bound on the error of the approximation $u_{\mathcal{G}}$

$$\|u - u_{\mathcal{G}}\|_{H^1(Q)} \leq Cd|u|_{H^2(Q)},$$

is proven in [4]. Here, d denotes the maximal distance between neighboring inclusions. Such an a priori result shows the potential of the new approach but it is only the very first step. Besides considering the 3-dimensional version of problem (3) and its approximation, which is rather straight forward, more general geometries with regard to the inclusions and more general differential equations need to be studied. Furthermore, the model needs to be investigated with respect to its asymptotic behavior regarding volume fraction and the interparticular distance.

References

[1] Leonid Berlyand, Yuliya Gorb, and Alexei Novikov. Discrete network approximation for highly-packed composites with irregular geometry in three dimensions. In *Multiscale methods in science and engineering*, volume 44 of *Lect. Notes Comput. Sci. Eng.*, pages 21–57. Springer, Berlin, 2005.

[2] Leonid Berlyand and Alexander Kolpakov. Network approximation in the limit of small interparticle distance of the effective properties of a high-contrast random dispersed composite. *Arch. Ration. Mech. Anal.*, 159(3):179–227, 2001.

[3] Leonid Berlyand and Alexei Novikov. Error of the network approximation for densely packed composites with irregular geometry. *SIAM J. Math. Anal.*, 34(2):385–408 (electronic), 2002.

[4] Daniel Peterseim. Finite Element analysis of randomly dispersed composites. Preprint in preparation, 2009.

Exact sampling for highly oscillatory molecular systems

Petr Plecháč

(joint work with Mathias Rousset)

We present a new numerical method called *implicit mass-matrix penalization* (IMMP) for numerical integration and sampling large particle systems whose dynamics exhibits multiple time scales. The detailed description and numerical analysis of the IMMP method can be found in [PleRous].

In this contribution we describe the IMMP method applied to Langevin processes (Hamiltonian dynamics with stochastically perturbed forces) in order to obtain an efficient and accurate sampling from the *canonical distribution* at the inverse temperature $\beta = 1/kT$ associated with the separable Hamiltonian $H(p,q) = \frac{1}{2}p^T M^{-1} p + V(q)$. The potential is assumed to be of form $V(q) = U(q, \xi(q))$ with the "fast" degrees of freedom (fDOFs) $(\xi_1, .., \xi_n)$ explicitly given, and $q \in \mathbb{R}^d$,

$p \in \mathbb{R}^d$. The knowledge of "fast forces" is not required, and the variables ξ can be chosen arbitrarily. If the fDOFs are not identified the method retains its approximation properties while not performing efficiently. The method also provides a good approximation at large temporal scales of the dynamical behavior of the system.

The IMMP method does not aim at resolving highly oscillatory behaviour (see, e.g., a review [PP1]) neither it introduces rigid constraints for oscillatory degrees of freedom ([PP5]). Instead the method replaces direct constraints by implicit mass-matrix penalization, which integrates fDOFs, but with a tunable mass penalty. The method designed in this way achieves the two goals: (i) from the dynamical point of view, the IMMP method amounts to an appropriate interpolation between exact dynamics and constrained dynamics considered in the second family of the methods mentioned above. Moreover, a freely tunable trade-off between dynamical modification and stability is obtained; (ii) from the sampling point of view, the IMMP dynamics preserves the canonical equilibrium distribution, up to time step errors and an easily computable geometric correcting potential. This leads to Metropolis Monte Carlo methods that sample *exactly* the canonical distribution. When using Metropolis schemes, the forces arising from the geometric correcting potential need not be computed.

Implicit mass-matrix penalization method. The fDOFs are penalized with a mass-tensor modification given by $M_\nu(q) = M + \nu^2 \nabla_q \xi \, M_z \, \nabla_q^T \xi$, where ν denotes the penalty intensity, and M_z a "virtual" mass matrix associated with the fDOFs. The position dependence of the mass-penalization introduces a geometric bias. This bias is corrected by introducing an effective potential $V_{\mathrm{fix},\nu}(q) = \frac{1}{2\beta} \ln\left(\det\left(M_\nu(q)\right)\right)$, which turns out to be a ν^{-1}-perturbation of the usual Fixman corrector (see [PP3]) associated with the sub-manifold defined by constraining the fDOFs ξ. The key point is then to use an implicit representation of the mass penalty with the aid of the extended Hamiltonian $H_{\mathrm{IMMP}}(p, p_z, q, z) = \frac{1}{2} p^T M^{-1} p + \frac{1}{2} p_z^T M_z^{-1} p_z + V(q) + V_{\mathrm{fix},\nu}(q)$, together with the constraint $\xi(q) = \frac{z}{\nu}$. The auxiliary degrees of freedom z are endowed with the "virtual" mass-matrix M_z. The constraints (C_ν) are applied in order to identify the auxiliary variables and the fDOFs ξ with a coupling intensity tuned by ν. The typical time scale of the fDOFs is thus enforced by the penalty ν. The system is coupled to a thermostat through a Langevin equation, which yields a stochastically perturbed dynamics that samples the equilibrium canonical distribution. As it was shown in [PleRous] the method has the following desirable properties: (i) the associated canonical equilibrium distribution in position is independent of the penalty ν; (ii) the limit of vanishing penalization ($\nu = 0$) is the original full dynamics, enabling the construction of dynamically consistent numerical schemes, (iii) the limit of infinite penalization is a standard effective constrained dynamics on the "slow" manifold associated with stiff constraints on ξ; (iv) numerical integrators can be obtained through a simple modification of standard integrators for effective dynamics with constraints yielding equivalent computational complexity.

When the system is thermostatted, i.e., kept at the constant temperature, the long time distribution of the system in the phase-space is given by the canonical equilibrium measure at the inverse temperature β (also called the NVT distribution) given by $\mu(dp\,dq) = \frac{1}{Z}e^{-\beta H(p,q)}dp\,dq$ with the normalization constant $Z < \infty$. The standard dynamics used to model thermostatted systems are given by Langevin processes. The stochastically perturbed equations of motion of the Langevin type define the dynamics with implicit mass-matrix penalization.

Definition 0.1 (IMMP,[PleRous]). *The implicit Langevin process* $\{q_t, z_t, p_t, (p_z)_t\}_{t\geq 0}$ *associated with Hamiltonian* H_{IMMP} *and constraints* (C_ν) *is defined by the following equations of motion*

$$
(1)\qquad \begin{cases} \dot{q} = M^{-1}p \\ \dot{z} = M_z^{-1}p_z \\ \dot{p} = -\nabla_q V(q) - \nabla_q V_{\mathrm{fix},\nu}(q) - \gamma\dot{q} + \sigma\dot{W} - \nabla_q\xi\,\dot{\lambda} \\ \dot{p}_z = -\gamma_z\dot{z} + \sigma_z\dot{W}_z + \dfrac{\dot{\lambda}}{\nu} \\ \xi(q) = \dfrac{z}{\nu}\,, \qquad\qquad (C_\nu) \end{cases}
$$

The process $\{W_t\}_{t\geq 0}$ *(resp.* $\{(W_z)_t\}_{t\geq 0}$ *) is a standard multi-dimensional white noise,* γ *(resp.* γ_z*) a* $d\times d$ *(resp.* $n\times n$*) non-negative symmetric dissipation matrix,* σ *(resp.* σ_z*) is the fluctuation matrix satisfying* $\sigma\sigma^T = \frac{2}{\beta}\gamma$ *(resp.* $\sigma_z\sigma_z^T = \frac{2}{\beta}\gamma_z$*). The process* $\{\lambda_t\}_{t\geq 0} \in \mathbb{R}^n$ *compose the Lagrange multipliers associated with the constraints* (C_ν) *and adapted with the white noise.*

This process is naturally equivalent to the explicit mass-penalized Langevin process in $\mathbb{R}^d \times \mathbb{R}^d$ associated with M_ν. Moreover, when the penalization vanishes ($\nu \to 0$), the evolution law of the process $\{p_t, q_t\}_{t\geq 0}$ or $\{(p_\nu)_t, q_t\}_{t\geq 0}$ converges towards the original dynamics. By construction, statistics of positions q of the mass penalized Hamiltonian are independent of the penalization, leading to the *exact canonical statistics* in position variables.

Numerical schemes. The key ingredient for achieving efficient numerical simulation is to use an integrator that enforces the constraints associated with the implicit formulation of the mass penalized dynamics (1). The mass-penalization introduced here may then be considered as a special method of pre-conditioning for a stiff ODE system with an "implicit", in the time evolution sense, structure. Here, the "implicit" structure amounts to solving the imposed constraints $\xi(q) = z/\nu$ in (1). As an example of numerical schemes we present IMMP with the classical leapfrog/Verlet scheme that enforces constraints, usually called RATTLE, see, e.g., [PP2] for numerical methods for constrained mechanical systems.

Scheme 0.1 ([PleRous]). *Dynamical integrator:*

Step 1: *Integrate the Hamiltonian part with:*

$$
\left\{
\begin{array}{l}
p_{n+1/2} = p_n - \dfrac{\delta t}{2}(\nabla_q V + \nabla_q V_{\mathrm{fix},\nu})(q_n) - \nabla_q \xi(q_n)\lambda_{n+1/2} \\
p^z_{n+1/2} = p^z_n + \dfrac{1}{\nu}\lambda_{n+1/2}
\end{array}
\right.
$$

$$
\left\{
\begin{array}{l}
q_{n+1} = q_n + \delta t M^{-1} p_{n+1/2} \\
z_{n+1} = z_n + \delta t M_z^{-1} p^z_{n+1/2}
\end{array}
\right.
$$

$$
\xi(q_{n+1}) = \frac{z_{n+1}}{\nu} \qquad (C_{1/2})
$$

$$
\left\{
\begin{array}{l}
p_{n+1} = p_{n+1/2} - \dfrac{\delta t}{2}(\nabla_q V + \nabla_q V_{\mathrm{fix},\nu})(q_{n+1}) - \nabla_q \xi(q_{n+1})\lambda_{n+1} \\
p^z_{n+1} = p^z_{n+1} + \dfrac{1}{\nu}\lambda_{n+1}
\end{array}
\right.
$$

$$
\nabla_q^T \xi(q_{n+1})\, M^{-1} p_{n+1} = \frac{1}{\nu} M_z^{-1} p^z_{n+1} \qquad (C_1)\,. \tag{2}
$$

Step 2: *Integrate if necessary the Gaussian fluctuation/dissipation part with a mid-point Euler scheme with constraints.*

For accurate sampling of the equilibrium distribution, a Metropolis acceptance, rejection time-step corrector can be added at each time step of the deterministic integrator leading to Generalized Hybrid Monte Carlo (GHMC) ([PP4]).

Scheme 0.2 ([PleRous])**.** *The IMMP algorithm with Metropolis correction:*

Step 1: *Compute* $(q_{n+1}, z_{n+1}, p_{n+1}, p^z_{n+1})$ *with the integrator* (2)*, and set*

$$
\Delta H_{n+1} = H_{\mathrm{IMMP}}(q_{n+1}, z_{n+1}, p_{n+1}, p^z_{n+1}) - H_{\mathrm{IMMP}}(q_n, z_n, p_n, p^z_n)\,.
$$

If $(q_{n+1}, z_{n+1}, p_{n+1}, p^z_{n+1})$ *does not belong to* $D_{\delta t}$*, set* $\Delta H_{n+1} = +\infty$*.*

Step 2: *Accept the step with the probability* $\min(1, e^{-\beta \Delta H_{n+1}})$*, otherwise reject, flip momenta, and set*

$$
(q_{n+1}, z_{n+1}, p_{n+1}, p^z_{n+1}) = (q_n, z_n, -p_n, -p^z_n)\,.
$$

Step 3: *Integrate the Gaussian fluctuation/dissipation part with a mid-point Euler scheme.*

The efficiency of the IMMP method as compared to the Verlet/Leapfrog integrator is quantified from two different viewpoints.
Dynamics. The critical time step $\delta t_c^{\mathrm{dyn}}$ is defined in such a way that it measures the average largest time step for which the scheme is stable.
Sampling. When using a Metropolis correction step in the numerical simulation, as in Scheme 0.2, the critical time step is correlated to the rejection rate of the Metropolis step, since the larger the former is, the more rejections will occur. Thus for sampling methods, the time step $\delta t_c^{\mathrm{sampl}}$ is tuned in order to achieve a given rate of rejection ρ.

A systematic comparison of the efficiency is presented in [PleRous] where the method is applied to N-alkane chains. As the number N of atoms in the alkane

chain increases the dynamics exhibit larger and larger number of oscillatory time scales. The numerical investigation has demonstrated that the IMMP method allows for increased critical time steps $\delta t_c^{\rm dyn}$ and $\delta t_c^{\rm sampl}$ while, at the same time, the dynamical and statistical properties of the system are approximated. The improved stability properties of the IMMP time integration algorithm have been proved rigorously for the harmonic chain. In particular, it has been shown that if ν is properly scaled with the size of the system N the critical time steps can increase with the size of the system. Such property does not hold for the Verlet/Leapfrog scheme where the increasing size of the system requires decreasing integration time steps. Furthermore, convergence to equilibrium distribution has been investigated numerically and it has been observed that the decorrelation time for N-alkane chains decreases with the size of the system N if the penalty ν is scaled with the size of the system, see [PleRous].

Acknowledgment: The research of M.R. was partially supported by the EPSRC grant GR/S70883/01 while he was visiting Mathematics Institute, University of Warwick. The research of P.P. was partially supported by the National Science Foundation under the grant NSF-DMS-0813893 and by the Office of Advanced Scientific Computing Research, U.S. Department of Energy; the work was partly done at the ORNL, which is managed by UT-Battelle, LLC under Contract No. DE-AC05-00OR22725.

References

[PleRous] P. Plecháč and M. Rousset. Implicit mass-matrix penalization of hamiltonian dynamics with application to exact sampling of stiff systems. accepted in *SIAM Multiscale Modeling and Simulations*, 2009.

[PP1] D. Cohen, T. Jahnke, K. Lorenz, and Ch. Lubich. Numerical integrators for highly oscillatory Hamiltonian systems: a review. In Aexander Mielke, editor, *Analysis, Modeling and Simulation of Multiscale Problems*, pages 553–576. Springer, 2006.

[PP2] C. Lubich E. Hairer, G. Wanner. *Geometric Numerical Integration, Structure-Preserving Algorithms for Ordinary Differential Equations*. Springer, 2002.

[PP3] M. Fixman. Simulation of polymer dynamics. I. General theory. *J. Chem. Phys.*, 69:1527, 1978.

[PP4] A. M. Horowitz. A generalized guided Monte Carlo algorithm. *Phys. Lett.B*, 268:247–252, 1991.

[PP5] S. Reich and B. Leimkuhler. *Simulating Hamiltonian Dynamics*, volume 14 of *Cambridge Monographs on Applied and Computational Mathematics*. Cambridge University Press, 2005.

Adaptive Multiscale Modeling using Numerical Homogenization

Serge Prudhomme

(joint work with C. Jhurani, L. Demkowicz, J.T. Oden, and P.T. Bauman)

Modeling of engineering systems involving complex heterogeneous material structures at the nanoscale has emerged as an important research area. One application we are interested in is the analysis and modeling of mechanical properties of polymer structures created during the Step and Flash Imprint Lithography (SFIL) nanomanufacturing process. SFIL is a novel imprint lithography process designed

to transfer circuit patterns for fabricating microchips in low-pressure and room-temperature environments as schematically described by the right diagram of Figure 1. Since the smallest features in SFIL are only a few molecules across, as shown in the left picture of Figure 1, approximating them as a continuum is not completely accurate. Previous research on this subject has dealt with coupling discrete models with continuum hyperelasticity models (see e.g. [1, 2, 3, 4]). Simulation of the post-polymerization step actually requires the solution of large nonlinear energy minimization problems with fast spatial variation in material properties. An equilibrium configuration is found by minimizing the energy of a heterogeneous polymeric lattice model. Numerical solution of such a molecular statics base model, which is assumed to describe the microstructure completely, is computationally very expensive. This is due to the problem size on the order of millions of degrees of freedom. Rapid variation in material properties, ill-conditioning, nonlinearity, and non-convexity make this problem even more challenging to solve.

An alternative approach to the atomic-to-continuum coupling method is developed in this work for efficient approximation of the equilibrium solution. The main idea of the proposed approach relies on combining numerical homogenization, adaptive meshes, and goal-oriented error estimation. Traditionally, a finite element mesh is designed after obtaining material properties in different regions. In the current approach, however, we generate a sequence of coarse meshes and homogenize material properties on each coarse mesh element using a locally posed constrained convex quadratic optimization problem (see Figure 2). Upscaling is done using Moore-Penrose pseudoinverse of the linearized fine-scale element stiffness matrices and a material independent interpolation operator. Using an adjoint solution, we compute local error estimates with respect to quantities of interest, following the methodology described in e.g. [6, 7]. The error estimates also drive the automatic mesh adaptivity algorithm. Numerical results show that this method uses orders of magnitude fewer degrees of freedom to give fast and accurate approximate solutions of the original fine-scale problem. Critical to the computational speed of local homogenization is computing the pseudoinverse of rank-deficient matrices without using Singular Value Decomposition. To this end, we compare four algorithms, each having different desirable features. The algorithms are based on Tikhonov regularization, sparse QR factorization, a priori knowledge of the null-space of the matrix, and iterative methods based on proper splittings of matrices. These algorithms can exploit sparsity and thus are fast. We apply the new approach to a three-dimensional model that depicts part of a SFIL lattice with rectangular features for imprinting. It consists of approximately 13000 unit cells and 38000 degrees of freedom. The quantity of interest is the distance between the two vertical blocks at the base of the features. The initial mesh, consisting of 120 bi-linear elements, is shown on the left of Figure 3 while the final configuration following seven refinement iterations is shown on the right of the figure.

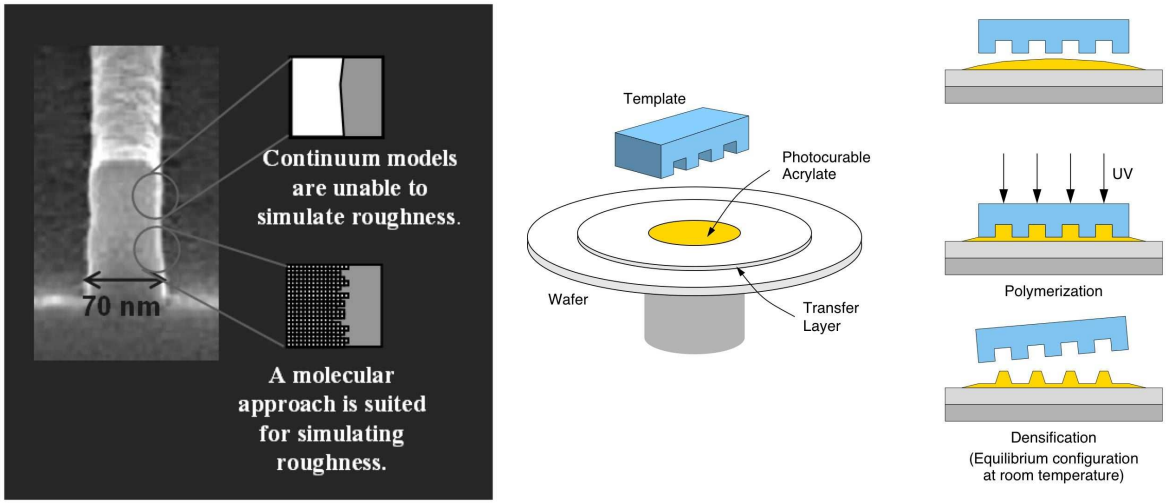

FIGURE 1. (Left) Polymeric microstructure obtained by the SFIL process as seen using a scanning electron microscope. (Right) A diagram of the SFIL process (not to scale).

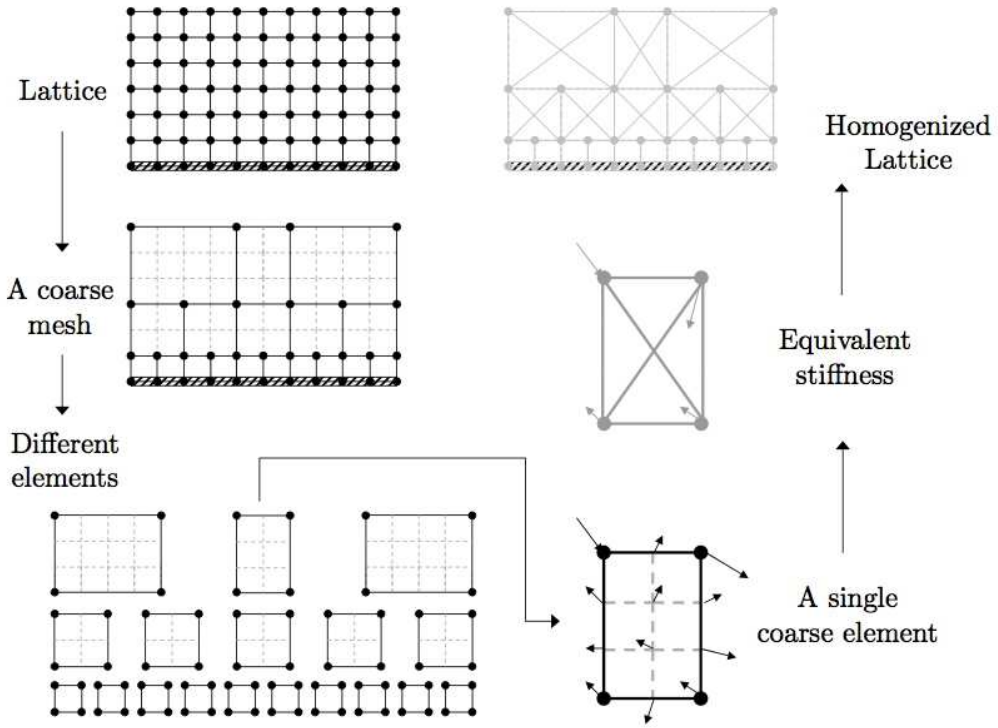

FIGURE 2. A 2-D lattice with fixed bottom layer is approximated with a coarse mesh. Effective local stiffness is computed on coarse elements and used to create a global effective lattice.

REFERENCES

[1] P.T. Bauman, H. Ben Dhia, N. Elkhodja, J.T. Oden, and S. Prudhomme, *On the application of the Arlequin method to the coupling of particle and continuum Models*, Computational Mechanics **42** (2008), 511–530 .

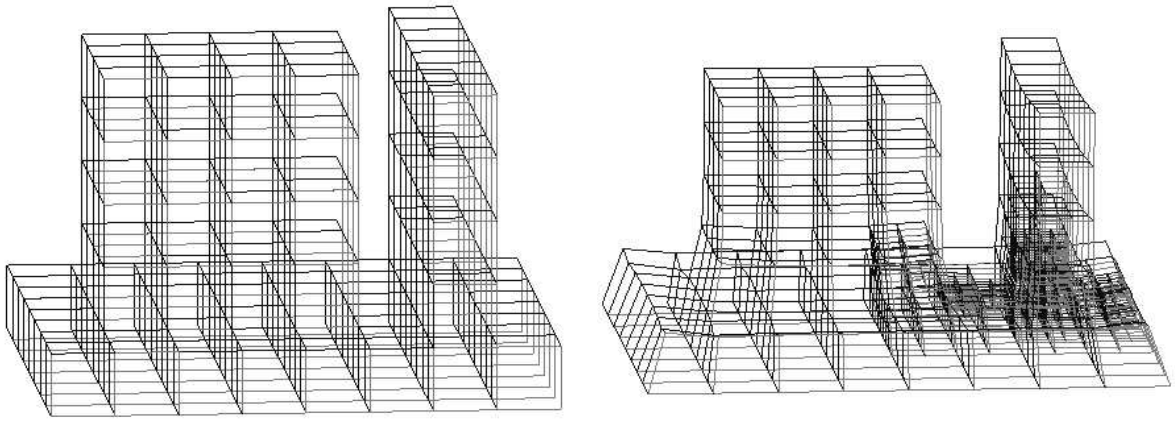

FIGURE 3. (Left) Initial mesh consisting of 120 bi-linear elements for a three-dimensional SFIL lattice model. (Right) Geometry at equilibrium and adapted configuration after seven refinement iterations.

[2] S. Prudhomme, H. Ben Dhia, P.T. Bauman, N. Elkhodja, and J.T. Oden, *On the application of the Arlequin method to the coupling of particle and continuum models*, Computer Methods in Applied Mechanics and Engineering **197** (2008), 3399–3409.
[3] P.T. Bauman, J.T. Oden, and S. Prudhomme, *Adaptive multiscale modeling of polymeric materials: Arlequin coupling and goals algorithms*, Computer Methods in Applied Mechanics and Engineering **198** (2009), 799–818.
[4] S. Prudhomme, L. Chamoin, H. Ben Dhia, and P.T. Bauman, *An adaptive strategy for the control of modeling error in two-dimensional atomic-to-continuum coupling simulations*, Computer Methods in Applied Mechanics and Engineering **198** (2009), 1887–1901.
[5] C. Jhurani, *Multiscale Modeling Using Goal-oriented Adaptivity and Numerical Homogenization*, Ph.D. Dissertation, The University of Texas at Austin (2009).
[6] J.T. Oden and S. Prudhomme, *Estimation of modeling error in computational mechanics*, J. Comput. Phys. **182** (2002), 496–515.
[7] S. Prudhomme, P.T. Bauman, and J.T. Oden, *Error control for molecular statics problems*, Int. J. Multiscale Comp. Eng. **4** (2006), 647-662.

A seamless multiscale method and its application to complex fluids

WEIQING REN

I will present a seamless multiscale method for the study of multiscale problems. The multiscale method aims at capturing the macroscale behavior of the system which is modeled by a (incomplete) macroscale model. This is done by coupling the macro model with a micro model: The macro model provides the necessary constraint for the micro model and the micro model supplies the missing data (e.g. the constitutive relation or the boundary conditions) needed in the macro model. In the multiscale method, the macro and micro models evolve simultaneously using different time steps, and they exchange data at every step. The micro model uses its own appropriate (micro) time step. The macro model uses a macro time step but runs at a slower pace than required by accuracy and stability considerations in

order for the micro dynamics to have sufficient time to adapt to the environment provided by the macro state. The method has the advantage that it does not require the reinitialization of the micro model at each macro time step or each macro iteration step. The data computed from the micro model is implicitly averaged over time. In this talk, I will discuss the algorithm of the multiscale method, the error analysis, and its application to complex fluids. If time allows, I will also discuss the stability of different coupling schemes in domain-decomposition type of multiscale methods.

Computational approaches to rate-independent processes: via Γ-convergence to multiscale modelling

Tomáš Roubíček

This contribution addresses the quasistatic initial-value problem for the following equality/inclusion:

$$\partial_u \mathcal{E}(t,u,z) = 0, \tag{1a}$$

$$\partial \mathcal{R}\Big(\frac{\mathrm{d}z}{\mathrm{d}t}\Big) + \partial_z \mathcal{E}(t,u,z) \ni 0, \tag{1b}$$

$$z(0) = z_0, \tag{1c}$$

with $u \in \mathcal{U}$ a "fast" variable, $z \in \mathcal{Z}$ an "slow" variable with an activated evolution, $\mathcal{U}$ and $\mathcal{Z}$ Banach spaces, $\mathcal{E} : [0,T] \times \mathcal{U} \times \mathcal{Z} \to \mathbb{R} \cup \{\infty\}$ a stored-energy potential, $\mathcal{R} : \mathcal{Z} \to \mathbb{R}^+ \cup \{\infty\}$ a convex (positively) homogeneous degree-1 dissipation pseudopotential, "∂" denoting (partial) subdifferentials or Gâteaux differentials. Due to the mentioned homogeneity degree-1, the problem (1) is rate independent in the sense that any monotone rescaling of time scale does not influence its (set of) solution(s). We will briefly refer to (1) as the $(\mathcal{U}\times\mathcal{Z}, \mathcal{E}, \mathcal{R}, z_0)$-problem.

If also $\mathcal{E}(t,\cdot,\cdot)$ is convex, the usual definition of weak solution to (1) is essentially equivalent (for details see [7]) to the so-called *energetic formulation*, i.e. (1c) is accompanied by the *energy equality* and *stability*:

$$\mathcal{E}\big(T,u(T),z(T)\big) + \mathrm{Var}_{\mathcal{R}}(z;0,T) = \mathcal{E}\big(0,u_0,z_0\big) + \int_0^T \partial_t \mathcal{E}(t,u(t),z(t))\,\mathrm{d}t, \tag{2a}$$

$$\forall v \in \mathcal{Z},\quad t \in [0,T]: \qquad \mathcal{E}\big(t,u(t),z(t)\big) \le \mathcal{E}\big(t,u(t),v\big) + \mathcal{R}\big(v-z(t)\big) \tag{2b}$$

with $\mathrm{Var}_{\mathcal{R}}(z;0,T)$ denoting the variation of $z : [0,T] \to \mathcal{Z}$ with respect to $\mathcal{R}$ defined as $\sup_{0\le t_0<t_1<\ldots<t_I\le T} \sum_i \mathcal{R}(z(t_i)-z(t_{i-1}))$. The energetic formulation (2), invented by Mielke at al. [13, 14], works also in the nonconvex case, is derivative-free, and expresses a competition between minimization of stored energy and maximization of dissipation. This is an applicable concept for a lot of activated processes occurring in mechanics (as plasticity, damage, phase transformation, or also e.g. ferromagnetics or ferroelectrics).

Energetic solutions can be obtained by limiting a time step $\tau\downarrow 0$ in the implicit time discretization of (1) provided its solutions are obtained by solving recursively

for $k=1,...,T/\tau$ the *global-optimization* problem:

$$\text{(3)}\quad \text{Minimize}\quad \mathcal{E}(k\tau,u_\tau^k,z_\tau^k)+\mathcal{R}(z_\tau^k-z_\tau^{k-1})\quad\text{subject to}\quad (u_\tau^k,z_\tau^k)\in\mathcal{U}\times\mathcal{Z}$$

with $z_\tau^0=z_0$ from (1c). Important phenomenon related with rate-independency is that, for any $1\le K\le T/\tau$, the following *two-sided energy estimate* holds:

$$\text{(4)}\quad \sum_{k=0}^{K}\partial_t\mathcal{E}_\tau\big(t,u_\tau^k,z_\tau^k\big)\,\mathrm{d}t\le\mathcal{E}\big(K\tau,u_\tau^K,z_\tau^K\big)-\mathcal{E}\big(0,u_0,z_0\big)+\mathrm{Var}_{\mathcal{R}}\big(z_\tau;0,K\tau\big)\le\sum_{k=0}^{K}\partial_t\mathcal{E}_\tau\big(t,u_\tau^{k-1},z_\tau^{k-1}\big)\,\mathrm{d}t,$$

where z_τ is the piece-affine interpolant of the values $(z_\tau^0,z_\tau^1,z_\tau^2,...,z_\tau^K)$. Violation of (4) indicates a failure of an optimization algorithm solving (3), and it may be exploited to return back to previous time level(s) and to optimize the objective in (4) with a different initial guess, typical this one which was unsuccessfully obtained in subsequent time levels. This *energy-based backtracking*, devised and tested in [12] for a 2D damage problem (and later in [3] for 3D martensitic transformation), may generally qualitatively help in solving the recursive global optimization problem (3) which is very nontrivial in cases when $\mathcal{E}\big(t,\cdot,\cdot\big)$ is not convex.

Considering of sequences of functionals $\{\mathcal{E}_n\}_{n\in\mathbb{N}}$ and $\{\mathcal{R}_n\}_{n\in\mathbb{N}}$ that Γ-converge to $\mathcal{E}$ and $\mathcal{R}$, respectively, it has been observed in [11] that an essential condition for convergence of the energetic solutions of $(\mathcal{U}\times\mathcal{Z},\mathcal{E}_n,\mathcal{R}_n,z_0)$-problems is the *joint-recovery-sequence* condition, i.e. for any sequence $(t_n,u_n,z_n)\to(t,u,z)$ and for any $(\widetilde{u},\widetilde{z})\in\mathcal{U}\times\mathcal{Z}$, to find another sequence $\{(\widetilde{u}_n,\widetilde{z}_n)\}_{n\in\mathbb{N}}$ such that

$$\text{(5)}\quad \limsup_{n\to\infty}\big(\mathcal{E}(t_n,\widetilde{u}_n,\widetilde{z}_n)+\mathcal{R}(\widetilde{z}_n-z_n)-\mathcal{E}(t_n,u_n,z_n)\big)\le\mathcal{E}(t,\widetilde{u},\widetilde{z})+\mathcal{R}(\widetilde{z}-z)-\mathcal{E}(t,u,z).$$

Constructing explicitly joint recovery sequences $\{(\widetilde{u}_n,\widetilde{z}_n)\}_{n\in\mathbb{N}}$ thus represents the main task in limiting various problems in mechanics as, e.g., partial damage to a complete damage as in [4] or elastic delamination [5] to a Griffith-type brittle delamination as in [20].

Another prominent usage of Γ-convergence is a *relaxation* of $\mathcal{E}(t,\cdot,\cdot)$ in case of lack of its lower semicontinuity in any topology which would yield compact level sets. The sequence $\{\mathcal{E}_n\}$ can typically arise by some higher-gradient theory that vanishes with $n\to\infty$ and the minimizers typically develop a microstructure (often modelled by Young measures). Thus *multiscale* problems can effectively be solved on a "mesoscopical"-level in the relaxed form and simultaneously justified from a "microscopical"-level by higher-gradient-type regularizations. This concerns e.g. isothermal models of shape-memory alloys on microscopical level in [1, 15] limited to mesoscopical level [6, 9, 18], or models of micromagnetics in [22] limited to a mesoscopical level [19].

Numerical approximation can be simply fitted into this general scenario by considering $\{\mathcal{E}_n\}$ with $\mathrm{dom}\,\mathcal{E}_n(t,\cdot,\cdot)$ a finite-dimensional subspace of $\mathcal{U}\times\mathcal{Z}$ (dependent on n but not on t). Then combination with time-discretization (3) yields an efficient numerical strategy even for nonconvex problems if adopting the energy-based

backtracking strategy based on (4) with $\mathcal{E}_n$ and $\mathcal{R}_n$ in place of $\mathcal{E}$ and $\mathcal{R}$, respectively. Convergence of such numerical schemes can be proved [10] by a case-by-case explicit construction of joint recovery sequences. If $\mathcal{E}(t,\cdot,\cdot)$ is (not far from to be) quadratic, also rate-of-error estimates are at disposal [8].

A useful extension to rate-dependent systems hosting a rate-independent processes only as some sub-system has been devised in [16] by considering *inertial/viscosity* effects and, in [17], also full *thermodynamics*. For the latter extension in a particular case see also [21]. Although the technique of Γ-convergence and (5) can be adopted and modified to such situations too, any analog of (4) is lost, however. In the latter anisothermal case, also the variational structure leading to minimization problems like (3) is lost and some fixed-point arguments or numerical iterations are to replace the mere direct method, cf. [17] or also [2].

Acknowledgement: The support of this long-term research from the grants A 100750802 (GA AV ČR), MSM 21620839, LC 06052 (MŠMT ČR), 106/09/1573 and 201/09/0917 (GA ČR), and AV0Z20760514 (ČR) is acknowledged.

References

[1] M.Arndt, M.Griebel, T.Roubíček: Modelling and numerical simulation of martensitic transformation in shape memory alloys. *Continuum Mech. Thermodyn.* **15** (2003), 463-485.

[2] S.Bartels, T.Roubíček: Thermoviscoplasticity in isotropic materials undergoing thermal expansion. In preparation.

[3] B.Benešová: Modeling of shape-memory alloys on the mesoscopic level. Proc. Conf. *ESOMAT, Prague, 2009*, submitted.

[4] G.Bouchitté, A.Mielke, T.Roubíček: A complete damage problem at small strains. *Zeitschrift angew. Math. Phys.* **60** (2009), 205-236.

[5] M.Kočvara, A.Mielke, T.Roubíček: A rate-independent approach to the delamination problem. *Math. and Mech. of Solids* **11** (2006), 423-447.

[6] M.Kružík, A.Mielke, T.Roubíček: Modelling of microstructure and its evolution in shape-memory-alloy single-crystals, in particular in CuAlNi. *Meccanica* **40** (2005), 389-418.

[7] A.Mielke: Evolution of rate-independent systems. In: *Handbook of Differential Equations: Evolut. Diff. Equations.* (C.Dafermos, E.Feireisl, eds.) North-Holland, 2005, pp.461–559.

[8] A.Mielke, L.Paoli, A.Petrov, U.Stefanelli: Error estimates for space-time discretization of a rate-independent variational inequality. (Preprint no.1407, WIAS Berlin, 2009). Submitted.

[9] A.Mielke, T.Roubíček: A rate-independent model for inelastic behavior of shape-memory alloys. *Multiscale Modeling and Simulation* **1** (2003), 571-597.

[10] A.Mielke, T.Roubíček: Numerical approaches to rate-independent processes and applications in inelasticity. *Math. Modelling Numer.Anal.* **43** (2009), 395-428.

[11] A.Mielke, T.Roubíček, U.Stefanelli: Γ-limits and relaxations for rate-independent evolutionary problems. *Calc. Var. P.D.E.* **31** (2008), 387-416.

[12] A.Mielke, T.Roubíček, J.Zeman: Complete damage in elastic and viscoelastic media and its energetics. *Comp. Methods Appl. Mech. Engr.*, to appear.

[13] A.Mielke, F.Theil: On rate-independent hysteresis models. *Nonlin. Diff. Eq. Appl.* **11** (2004) 151–189 (Accepted July 2001).

[14] A.Mielke, F.Theil, V.I.Levitas: A variational formulation of rate-independent phase transformations using an extremum principle. *Archive Rat. Mech. Anal.* **162** (2002) 137–177.

[15] K.R.Rajagopal, T.Roubíček: On the effect of dissipation in shape-memory alloys. *Nonlinear Anal., Real World Applications* **4** (2003), 581-597.

[16] T.Roubíček: Rate independent processes in viscous solids at small strains. *Math. Methods Appl. Sci.* **32** (2009), 825-862.

[17] T.Roubíček: Thermodynamics of rate independent processes in viscous solids at small strains. *SIAM J. Math. Anal.*, to appear.
[18] T.Roubíček, M.Kružík, J.Koutný: A mesoscopical model of shape-memory alloys. *Proc. Estonian Acad. Sci. Phys. Math.* **56** (2007), 146-154.
[19] T.Roubíček, M.Kružík: Microstructure evolution model in micromagnetics. *Zeit. für angew. Math. und Physik* **55** (2004), 159-182.
[20] T.Roubíček, L.Scardia, C.Zanini: Quasistatic delamination problem. *Continuum Mech. Thermodynam.*, in print.
[21] T.Roubíček, G.Tomassetti: Thermodynamics of shape-memory alloys under electric current. *Zeitschrift angew. Math. Phys.*, (2009), in print. DOI: 10.1007/s00033-009-0007-1
[22] T.Roubíček, G.Tomassetti, C.Zanini: The Gilbert equation with dry-friction-type damping. *J. Math. Anal. Appl.* **355** (2009), 453-468.

Equation-assisted methods for the coarse behaviour of kinetic equations

Giovanni Samaey
(joint work with Wim Vanroose, Mathias Rousset)

1. Introduction

In traditional modeling, one derives evolution equations at the (macroscopic, coarse) scale of interest; these are used to perform a variety of tasks (simulation, bifurcation analysis, optimization) using an arsenal of analytical and numerical techniques. For many complex systems, however, although one observes evolution at a macroscopic scale of interest, accurate models are only given at a more detailed (fine-scale, microscopic) level of description. Equation-free methods [8, 2, 3] bypass the derivation of coarse evolution equations when these equations conceptually exist but are not available in closed form. The main building block is a coarse time-stepper, which consists of three steps: (1) *lifting*, i.e., creation of initial conditions for the fine-scale model, conditioned upon the coarse state; (2) *simulation* using the fine-scale model; and (3) *restriction*, i.e., observation (estimation) of the coarse state. Coarse-scale solvers (e.g. projective integration or time-stepper based bifurcation tools) are then wrapped around this coarse time-stepper.

In many systems, however, an approximate coarse model has been derived in some sort of convenient limit. At first sight, it would appear that this knowledge is lost in the equation-free framework – a statement that is not true in general. In this abstract, we discuss two ways in which such approximate coarse models can increase efficiency and accuracy of equation-free computations. First we briefly review preconditioning of equation-free Newton–Krylov methods. Here, the approximate coarse model is used to construct the preconditioner, such that we can achieve fast Krylov convergence. This is illustrated on a lattice Boltzmann model for ionization in gases. Second, we discuss variance reduced simulations of a velocity-jump process for bacterial chemotaxis.

2. Preconditioning of equation-free Newton–Krylov methods

2.1. **Equation-free Newton Krylov methods.** A coarse steady state can be computed as a fixed point of the coarse time-stepper. While the corresponding Jacobian is not available, Jacobian-vector products can be estimated using repeated calls to the coarse time-stepper from nearby initial conditions, enabling the use of Krylov methods. The Krylov convergence rate depends heavily on the spectral properties of the Jacobian. For GMRES to converge rapidly, the eigenvalues should be clustered and bounded away from 0. However, the Jacobian of the fixed point nonlinear system always contains both eigenvalues close to 0 and close to 1. Hence, preconditioning will be necessary.

2.2. **Lattice Boltzmann model for streamer ionization fronts.** Streamers are sharp, non-linear waves of electrons that propagate through gases in the presence of strong electric fields. The strong field accelerates the electrons that then cause ionization reactions during the collisions with the neutral gas particles. This impact ionization reaction creates additional electrons that are, again, accelerated. This results in an avalanche at the tip of the wave front.

We consider a D1Q5 (five-speed) lattice Boltzmann model for the electron distributions, coupled to an equation for the evolution of the electric field, as proposed in [9]. The unavailable coarse equation would be a system of two coupled PDEs, one for the electron density and one for the electric field.

This model exhibits coarse traveling fronts with arbitrary speed $c \geq c^*$, where c^* is called the critical speed, which appear as steady states in comoving frame.

2.3. **Preconditioning of Krylov method.** In [9], a Chapman–Enskog expansion was performed to derive an approximate equation for the evolution of the electron density, which was used as a preconditioner in [7]. In [6], we avoided this derivation by preconditioning with an equivalent operator (an operator of the same type, of which the coefficients are merely chosen to obtain a good convergence rate and that does not necessarily admit the same type of solutions). We also analyzed the effects of time discretization in both the preconditioner and coarse time-stepper [5].

3. Variance reduced simulation of bacterial chemotaxis

3.1. **Models for bacterial chemotaxis.** We consider bacteria sensitive to the concentration of chemoattractant, using a slight modification of the model described in [1]. Bacteria move with a constant speed v (run), and change direction at random instances in time (tumble), in an attempt to move towards regions with high chemoattractant concentrations. We will describe this behavior by a velocity-jump process, in which the jump intensity depends on some internal state $y \in \mathbb{Y} \subset \mathbb{R}^n$. The internal state models the memory of the bacterium and is subject to an evolution mechanism driven by the chemoattractants concentrations $S(x)$, where x is the present position of the bacterium.

Alternatively, one can model the jump intensity to depend on the chemoattractant gradient directly, which leads to a simplified process that is exactly equivalent

to a kinetic equation; this will be called the control process here. In [4], we prove that, with an appropriate choice of parameters, and in an appropriate diffusive asymptotics, both processes approach the same advection-diffusion equation in the limit of vanishing bacterial velocity.

3.2. **Coupling between the two processes.** We will simulate the density of bacteria using an ensemble of N particles that evolve according to the process with internal state. The density can then computed via standard kernel density estimation. We will reduce the variance of this simulation by using the fact that there is a strong relation between the process with internal state and the control process. To this end, we will simulate both processes *using the same random numbers* to obtain a strong correlation between each pair of bacteria. The important point is that a deterministic solution $n^c(x,t)$ for the control process can be obtained much more easily. An improved estimate can then be obtained using the technique of control variables.

In [4], an analysis of this coupling is presented that justifies the choice of the control process. The paper also contains some simulation results.

Acknowledgements

The work that is outlined in this abstract is joint with Wim Vanroose and Yannis Kevrekidis (section 2) and Mathias Rousset (section 3). Part of this work was performed during a research stay of GS at SIMPAF (INRIA - Lille, France), whose hospitality is gratefully acknowledged. GS is a Postdoctoral Fellow of the Research Foundation – Flanders (FWO – Vlaanderen). This work was partially supported by the Research Foundation – Flanders through Research Project G.0130.03 and by the Interuniversity Attraction Poles Programme of the Belgian Science Policy Office through grant IUAP/V/22 (GS). The scientific responsibility rests with its authors.

References

[1] R. Erban and H.G. Othmer. From individual to collective behavior in bacterial chemotaxis. *SIAM Journal on Applied Mathematics*, 65(2):361–391, 2004.

[2] I.G. Kevrekidis, C.W. Gear, J.M. Hyman, P.G. Kevrekidis, O. Runborg, and C. Theodoropoulos. Equation-free, coarse-grained multiscale computation: enabling microscopic simulators to perform system-level tasks. *Comm. Math. Sciences*, 1(4):715–762, 2003. An earlier version can be obtained as physics/0209043 from arXiv.org.

[3] I.G. Kevrekidis and G. Samaey. Equation-free multiscale computation: algorithms and applications. *Annual Review on Physical Chemistry*, 60, 2009. In press.

[4] M. Rousset and G. Samaey. Individual-based models for bacterial chemotaxis and variance-reduced simulations. in preparation, 2009.

[5] G. Samaey and W. Vanroose. An analysis of equivalent operator preconditioning of equation-free Newton–Krylov computations. Submitted to SIAM Journal on Numerical Analysis, 2008.

[6] G. Samaey, W. Vanroose, and I.G. Kevrekidis. Equivalent operator preconditioning of equation-free Newton–Krylov computations: a lattice boltzmann example. in preparation, 2009.

[7] G. Samaey, W. Vanroose, D. Roose, and I.G. Kevrekidis. Newton-Krylov solvers for the equation-free computation of coarse traveling waves. *Computer Methods in Applied Mechanics and Engineering*, 197:3480–3491, 2008.

[8] C. Theodoropoulos, Y.H. Qian, and I.G. Kevrekidis. Coarse stability and bifurcation analysis using time-steppers: a reaction-diffusion example. In *Proc. Natl. Acad. Sci.*, volume 97, pages 9840–9845, 2000.

[9] W. Vanroose, G. Samaey, and P. Van Leemput. Coarse-grained analysis of a lattice Boltzmann model for planar streamer fronts. TW report 479, Dept. of Computer Science, K.U. Leuven. Available from http://www.cs.kuleuven.be/publicaties/rapporten/tw/TW479.abs.html, 2006.

Multiscale methods for simulating epitaxial growth and neuronal network dynamics

Yi Sun

The heterogeneous multiscale method (HMM) provides a unified framework for designing efficient numerical methods for problems with multiple scales [1]. When a macroscale model is not explicitly given or not accurate enough, HMM provides a general strategy for supplementing the missing data from an explicitly given microscale model. There are usually two coupling strategies in the data estimation procedure. It can either be performed on the "fly" in a concurrent coupling method, where the microscale and the macroscale models are linked together throughout the computation. Or, the estimation can be done in a pre-processing step as in a serial coupling method, in which the needed data depends on very few variables and can be pre-computed. We give two examples with these coupling strategies as follows.

In [2] we investigate a heterogeneous multiscale method for interface tracking and apply the technique to the simulation of epitaxial growth. Our method relies on an efficient concurrent coupling between macroscale and microscale models. It couples kinetic Monte-Carlo (KMC) simulations on the microscale with the island dynamics model based on the level set method and a diffusion equation on the macroscale. Our main interest is to capture the motion of the island boundary at the macroscopic level in the cases where the computed velocity of the boundary will require simulation on the microscale. We perform the numerical simulations for island growth and step edge evolutions on the macroscale domain while keeping the KMC modeling of the internal boundary conditions. Our goal is to get comparably accurate solutions at potentially lower computational cost than for full KMC simulations, especially for step flow problem. Figure 1 shows the HMM strategy and the comparison results between HMM and KMC. In [3], we also applied the concurrent coupling strategy for interface tracking of combustion fronts.

Future work in simulation of epitaxial growth contains several angles. One is to focus on the nucleation problem. We will perform KMC simulations in the microscale domains to find the criterion for determining whether the nucleation can occur or not on the macroscale. The second one is to include both irreversible and reversible cases, where in the latter case thermal detachment of atoms from island

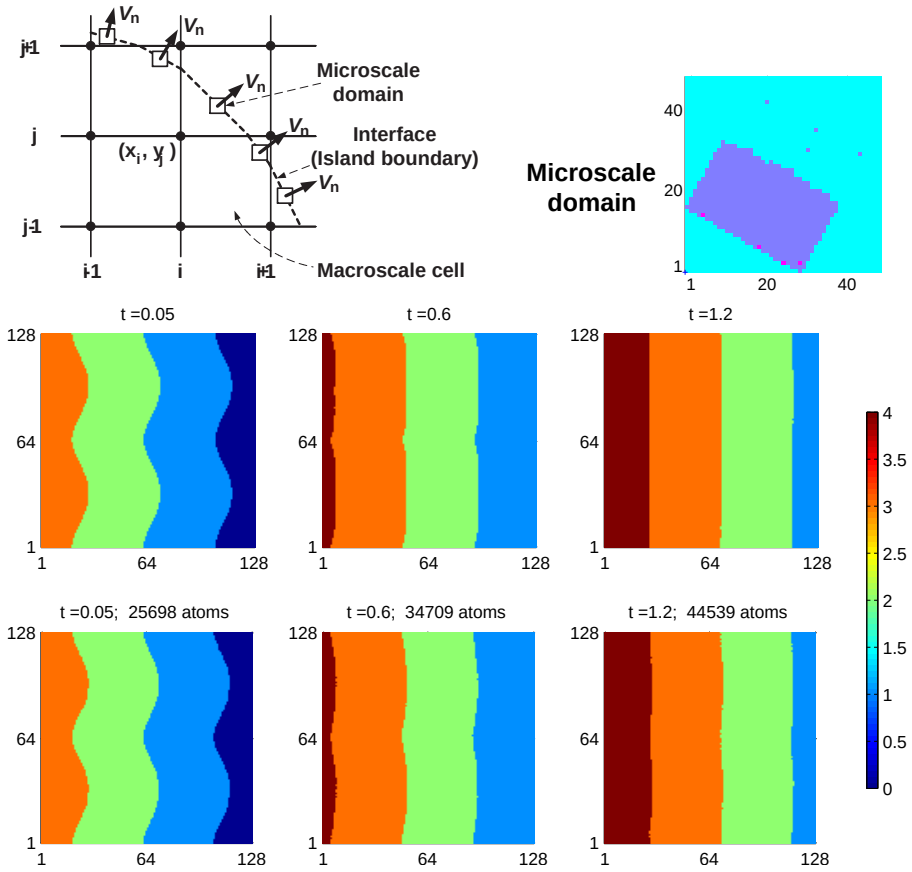

FIGURE 1. (Top left): In each macroscale cell which contains a segment of island boundaries, we set up a small box as the microscale domain. (Top right): A typical KMC simulation in a microscale domain. The dots in dark blue represent the atoms in the first layer and the dots in pink are the atoms in the second layer. (Middle): The evolution of the surface morphology in the HMM simulations during the total time of $t = 1.2$sec. (Bottom): The evolution of the surface morphology in the full KMC simulations. The locations of macroscale step edges from the HMM simulation match those of the full KMC result.

edges is allowed. One further direction is to deal with heteroepitaxial growth, where the effects of lattice mismatch and the strain relaxation must be incorporated.

For multiscale pre-computed strategy, we present an efficient library-based numerical method for simulating Hodgkin-Huxley (HH) neuronal networks in [4]. Our pre-computed high resolution data library contains typical neuronal trajectories (i.e., the time-courses of membrane potential and gating variables) during the interval of an action potential (spike) and it can allow us to avoid resolving the spikes in detail and to use large numerical time steps for evolving the HH neuron equations. By using the library-based method, we can evolve the HH networks

using time steps one order of magnitude larger than the typical time steps used for resolving the trajectories without the library, while achieving comparable resolution in statistical quantifications of the network activity. Moreover, our large time steps using the library method can break the stability requirement of standard ODE methods for the original dynamics. We compare our library-based method with Runge-Kutta (RK) methods, and find that our method can capture very well asynchronous, synchronous, and chaotic dynamics of HH neuronal networks. Figure 2 shows the comparison results.

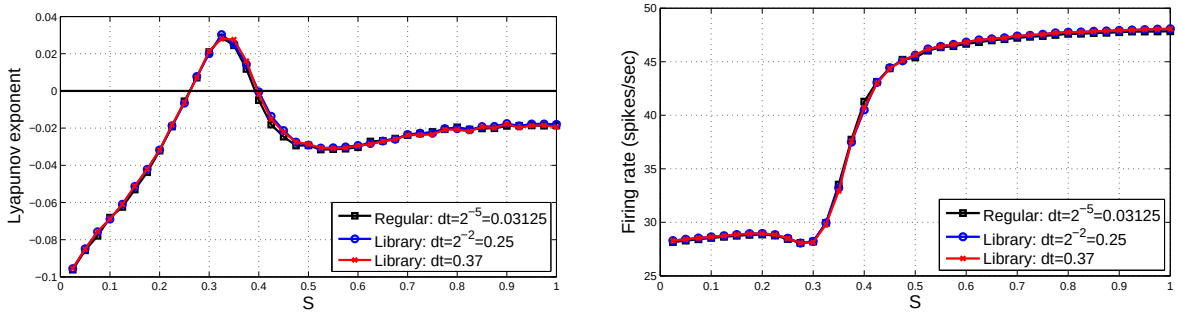

FIGURE 2. The comparison results of an all-to-all connected network of 100 HH neurons driven by Poisson spike inputs. (Left): Largest Lyapunov exponent of the network versus the coupling strengths S. The library method with large time steps can capture the chaotic regime ($0.26 < S < 0.39$) as well as the regular method does with a small time step. (Right): Average firing rate versus the coupling strength S. The library method can achieve more than 2 digits of accuracy using time steps 10 times larger than those used by the regular method for all values of S.

Future work with this multiscale pre-computed strategy will include the following. We will work with more complicated HH-like models which contain other ion channels and build the data library for the gating variables of these channels. It may also be applied to other biological networks which evolve stiff dynamics.

REFERENCES

[1] W. E and B. Engquist, *The heterogeneous multiscale methods*, Commun. Math. Sci. **1** (2003), 87–132.

[2] Y. Sun, R. Caflisch and B. Engquist, *A multiscale method for epitaxial growth*, under review in SIAM Multiscale Model. Simul. (2009)

[3] Y. Sun and B. Engquist, *Heterogeneous multiscale methods for interface tracking of combustion fronts*, SIAM Multiscale Model. Simul. **5** (2006), 532–563.

[4] Y. Sun, D. Zhou, A. V. Rangan and D. Cai, *Library-based numerical reduction of the Hodgkin-Huxley neuron for network simulations*, accepted in J. Comput. Neurosci. (2009)

Accuracy of Molecular Dynamics

Anders Szepessy

Born-Oppenheimer, Smoluchowski, Langevin and Ehrenfest dynamics are in this talk shown to be accurate approximations of time-independent Schrödinger observables for a molecular system, in the limit of large ratio of nuclei and electron masses, without assuming that the nuclei are localized to vanishing domains. The derivation, based on characteristics for the Schrödinger equation, bypasses the usual separation of nuclei and electron wave functions and gives a different perspective on initial and boundary conditions, caustics and irreversibility, the Born-Oppenheimer approximation, computation of observables, stochastic electron equilibrium states and symplectic numerical simulation in molecular dynamics modeling.

This extended abstract is a part of the introduction to the paper [1], where references to related work is included. The *time-independent Schrödinger* equation

$$H(x,X)\Phi(x,X) = E\Phi(x,X), \tag{1}$$

models nuclei-electron systems and is obtained from minimization of the energy in the solution space of wave functions. It is an eigenvalue problem for the energy $E \in \mathbb{R}$ of the system in the solution space, described by wave functions, $\Phi : \mathbb{R}^{3J} \times \mathbb{R}^{3N} \to \mathbb{C}$, depending on electron coordinates $x = (x^1, \ldots, x^J) \in \mathbb{R}^{3J}$, nuclei coordinates $X = (X^1, \ldots, X^N) \in \mathbb{R}^{3N}$, and a Hamiltonian operator $H(x,X)$

$$H(x,X) = V(x,X) - \frac{1}{2M}\sum_{n=1}^{N} \Delta_{X^n}.$$

The nuclei masses M are assumed to be large and the interaction potential V, independent of M, is in the canonical setting composed by the kinetic energy of electrons and Coulomb interaction of electrons and nuclei.

An essential feature of the partial differential equation (1) is the high computational complexity to determine the solution, in an antisymmetric/symmetric subset of the Sobolev space $H^1(\mathbb{R}^{3(J+N)})$. An attractive property of the Schrödinger equation (1) is the precise definition of the Hamiltonian and the solutions space, without unknown parameters. The agreement with measurements can be further improved by including relativistic and magnetic effects.

In contrast to the Schrödinger equation, a *molecular dynamics* model of nuclei $X : [0,T] \to \mathbb{R}^{3N}$, with a given potential $V_0 : \mathbb{R}^{3N} \to \mathbb{R}$, can be computationally studied also for large N by solving the ordinary differential equation

$$M\ddot{X}_\tau = -\partial_X V_0(X_\tau). \tag{2}$$

This computational and conceptual simplification motivates the study to determine the potential and its implied accuracy by a derivation of molecular dynamics from the Schrödinger equation, as started already in the 1920's with the seminal Born-Oppenheimer approximation. The purpose here is to contribute to the current understanding of such derivations, by showing improved convergence rates under new assumptions.

A useful sub step to derive molecular dynamics from the Schrödinger equation is *Ehrenfest dynamics*, for classical *ab initio* motion of the nuclei coupled to Schrödinger dynamics for the electrons,

$$
\begin{aligned}
M\ddot{X}_\tau^n &= -\int_{\mathbb{R}^{3J}} \phi_\tau^*(\cdot, X_\tau)\, \partial_{X^n} V(\cdot, X_\tau)\, \phi_\tau(\cdot, X_\tau)\, dx \\
i\dot{\phi}_\tau &= V(\cdot, X_\tau)\phi_\tau,
\end{aligned}
\tag{3}
$$

with the initial normalization $\int_{\mathbb{R}^{3J}} \phi_0^*(\cdot, X_0)\phi_0(\cdot, X_0)dx = 1$. The Ehrenfest dynamics (3) has been derived from the time-dependent Schrödinger equation through the self consistent field equations, by F.A. Bornemann and C. Schütte. Equation (3) can be used for *ab initio* computation of molecular dynamics. A next step is the Born-Oppenheimer approximation, where X_τ solves the classical *ab initio* molecular dynamics (2) with the potential $V_0 : \mathbb{R}^{3N} \to \mathbb{R}$ determined as an eigenvalue of the electron Hamiltonian $V(\cdot, X)$ for a given nuclei position X, that is $V(\cdot, X)\psi_0(X) = V_0(X)\psi_0(X)$, for instance with the electron ground state $\psi_0(X)$. The Born-Oppenheimer approximation has been derived from the time-dependent Schrödinger equation, first by G.A. Hagedorn.

The model (2) simulates dynamics at constant energy $M|\dot{X}|^2/2 + V_0(X)$, constant number of particles N and constant volume, i.e. the microcanonical ensemble. The alternative to simulate with constant number of particles, constant volume and constant temperature T, i.e. the canonical ensemble, is possible for instance with the stochastic *Langevin dynamics*

$$
\begin{aligned}
dX_\tau &= v_\tau d\tau \\
Mdv_\tau &= -\partial_X V_0(X_t)d\tau - Kv_t d\tau + (2TK)^{1/2} dW_\tau,
\end{aligned}
\tag{4}
$$

where W_τ is the standard Brownian process (at time τ) in $\mathbb{R}^{3N}$ with independent components and K is a positive friction parameter. When the observable only depends on the nuclei positions, i.e. not on the nuclei velocities or the correlation of positions at different times, the *Smoluchowski dynamics*

$$
dX_\tau = -\partial_X V_0(X_\tau) + (2T)^{1/2} dW_\tau \tag{5}
$$

is a simplified alternative to Langevin dynamics.

The work [1] derives the Ehrenfest dynamics (3) and the Born-Oppenheimer approximation from the time-independent Schrödinger equation (1) and the main point here is to establish improved convergence rates for molecular dynamics approximations of Scrödinger observables under simple assumptions.

The main idea in [1], inspired by work of N.F. Mott and J. Briggs & J.M. Rost, is to introduce the time-dependence from the classical characteristics in the Hamilton-Jacobi equation obtained by writing the time-independent eigenfunction (1) in WKB-form.

Two theorems in [1] present conditions for approximation of observables based on the Schrödinger equation by observables from the Ehrenfest dynamics and the Born-Oppenheimer dynamics with error $\mathcal{O}(M^{-1})$ respectively $\mathcal{O}(M^{-1/2})$, using that these approximate solutions generate approximate eigenstates to the

Schrödinger equation; studying this stability of the Schrödinger eigenvalue problem instead of perturbations of solution paths avoids the complications of accumulation of error on infinite time intervals. The derivation does not assume that the nuclei are supported on small domains; in contrast, derivations based on the time-dependent self consistent field equations require nuclei to be supported on small domains. The reason that small support is not needed here comes from the combination of the characteristics and sampling from an equilibrium density, that is, for large M the nuclei paths behave classically although they may not be supported on small domains. The derived approximations improve the previous $\mathcal{O}(M^{-1/2})$ rate for the Ehrenfest approximation the $\mathcal{O}(M^{-1/4})$ rate for the zero order Born-Oppeneheimer approximation. A remark in [1] relates the approximation results to the accuracy of symplectic numerical methods for molecular dynamics.

A section in [1] applies the Ehrenfest approximation result to derive the Langevin and Smoluchowski dynamics from the Ehrenfest dynamics, when the electron state is randomly perturbed from its ground state and the observable depends only on the nuclei positions but not their correlation at different time. The derivation uses a classical equilibrium Gibbs-Boltzmann distribution for the electron states and an assumption of a spectral gap, showing a theorem that observables of Langevin and Smoluchowski dynamics accurately approximate such Schrödinger observables. The main idea in the theorem is the non-standard view of a classical Gibbs-Boltzmann equilibrium distribution of electrons states, motivated by nuclei acting as heat bath for the electrons in the Ehrenfest Hamiltonian system.

References

[1] A. Szepessy, *Stochastic and deterministic molecular dynamics derived from the time-independent Schrödinger equation*, arXiv:0812.4338.

Strategies for the Finite Deformation Analysis of Microheterogeneous Media: Multiscale Aspects and Adaptivity

Peter Wriggers
(joint work with İlker Temizer)

Homogenization techniques allow an efficient and robust analysis of problems posed on highly heterogeneous bulk and interface topographies via the introduction of lower-scale models with predetermined constitutive behavior. The major steps in such techniques are (i) the construction of a homogenization methodology which extracts the behavior of the lower-scale model as reflected on the upper-scale and (ii) the definition of a homogenized problem that employs directly or indirectly the results of the homogenization methodology, the solution to which constitutes an approximation to the solution of the originally heterogeneous problem. Theoretically, the original heterogeneous primary solution field approaches the approximate homogenized one in the limit of a vanishingly small representative lower-scale dimension with respect to a representative upper-scale dimension. This convergence

behavior has been extensively studied based on the method of asymptotic expansions, particularly in the case of linearized constitutive behavior on periodically heterogeneous domains, as summarized recently in [1].

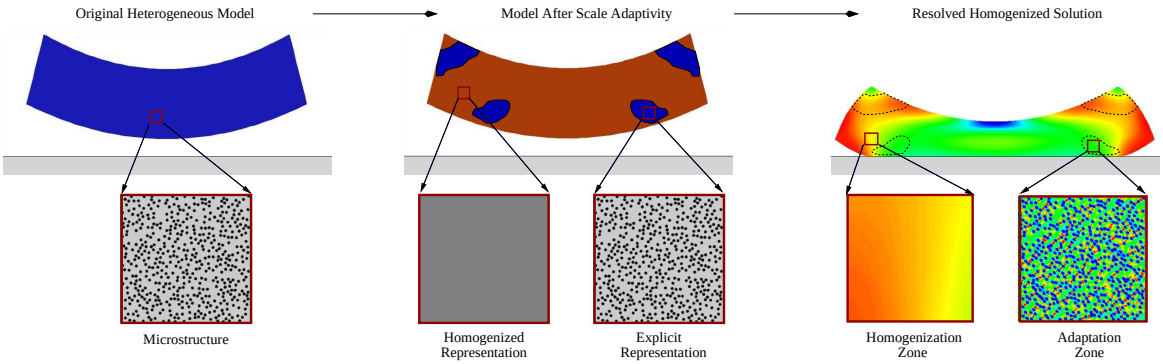

FIGURE 1. *The scale adaptation approach is depicted.*

In the context of purely mechanical bulk problems, which is the focus of this contribution, one is classically concerned with the analysis of a macrostructure with an underlying random or periodic microstructure. From an engineering perspective, many works have addressed the task of quantifying the degree of quality with which the original macroscale stress is approximated for such problems via homogenization techniques, and *scale adaptivity strategies* for improving the quality have been suggested where these methodologies perform below a desired level of accuracy. Sample typical situations of practical interest where the need for such strategies arise are regions near highly localized contact loads and the material interfaces in composites which are accompanied by high gradients in the solution fields associated with stress concentrations. Representative scale adaptivity strategies include [2, 3, 4].

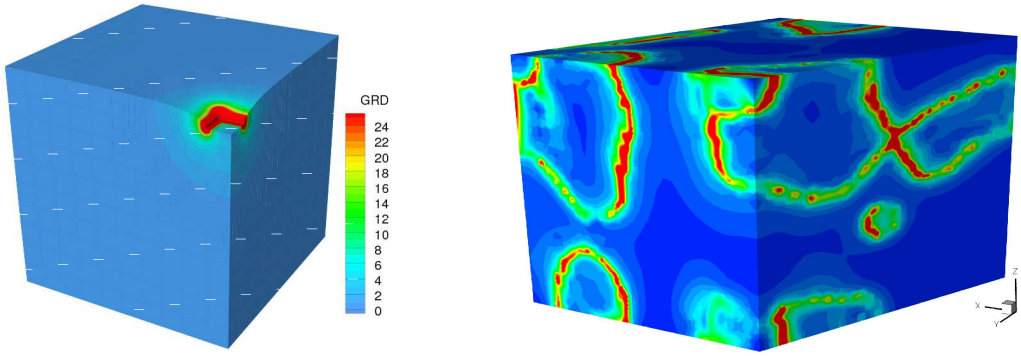

FIGURE 2. *Strain-gradient field distributions which demonstrate that critical zones are accompanied by severe gradients near concentrated contact loads (LEFT) and at material interfaces (RIGHT). Both figures employ the same scale.*

The scale adaptation technique that is of interest in this contribution employs an exact homogenized response in a preliminary analysis and subsequently reverts directly to an explicit microstructural model within designated critical zones to obtain a higher-order resolution of the microstructural response without introducing intermediate approximate models (Figure 1). Within this framework, the fundamental adaptation stage requires the computation of the *strain-gradient tensor* distribution, defined as $\mathbf{G} = \partial\mathbf{F}/\partial\mathbf{X}$ where $\mathbf{F}$ is the deformation gradient tensor distribution associated with the homogenized solution and $\mathbf{X}$ is the position vector in the reference configuration of the macrostructure. For this purpose, the *isoparameteric transform method* is employed which can estimate the gradients of cell-centered data with second-order accuracy on highly non-uniform and non-orthogonal meshes of quadrilateral and hexahedral elements [5]. Subsequently, motivated by the higher-order homogenization scheme in [6], adaptation zones where homogenization is deemed to perform below the desired accuracy are identified by monitoring the error quantity $||\mathbf{G}||L_{micro}$. When the error exceeds a given accuracy tolerance, significant variations in $\mathbf{F}$ takes place over length scales that are comparable to a representative microstructural dimension L_{micro}. This, however, is essentially a violation of the fundamental *separation of scales* assumption in homogenization. Consequently, the homogenized material description within these critical zones is replaced by the explicit microstructural representation and the solution of this scale-adapted model is recomputed. The adaptation zone size and shape is strongly influenced by microstructural parameters such as particle morphology and property mismatch ratios as well as by the magnitude of local loading conditions. The overall approach, which is summarized in Figure 3, remains tractable independent of the size of the microstructural features and is designed to deliver a locally improved solution quality. For more details, the interested reader is referred to [7] where efficient multiscale analysis methodologies based on homogenization are also summarized.

Future work will concentrate on aspects of quantifying solution quality improvement. This a particularly challenging task because small error tolerances induce large adaptation zones where localized homogenization errors are smoothed out, whereas large error tolerances induce smaller adaptation zones where homogenization does not perform accurately even in the absence of high strain-gradient magnitudes. Additionally, improvements towards the ability to handle thermoelastic microstructural response will be pursued in the finite deformation regime based on novel homogenization approaches together with the ability to incorporate random microstructures.

References

[1] G. A. Pavliotis, A. M. Stuart, *Multiscale Methods: Averaging and Homogenization*, Springer-Verlag (2008).

[2] J. Fish, K. Shek, *Multiscale analysis of composite materials and structures*, Composite Science and Technology **60** (2000), 2547–2556.

[3] A. Romkes, J. T. Oden, K. Vemaganti, *Multi-scale goal-oriented adaptive modeling of random heterogeneous materials*, Mechanics of Materials **38** (2006), 859–872.

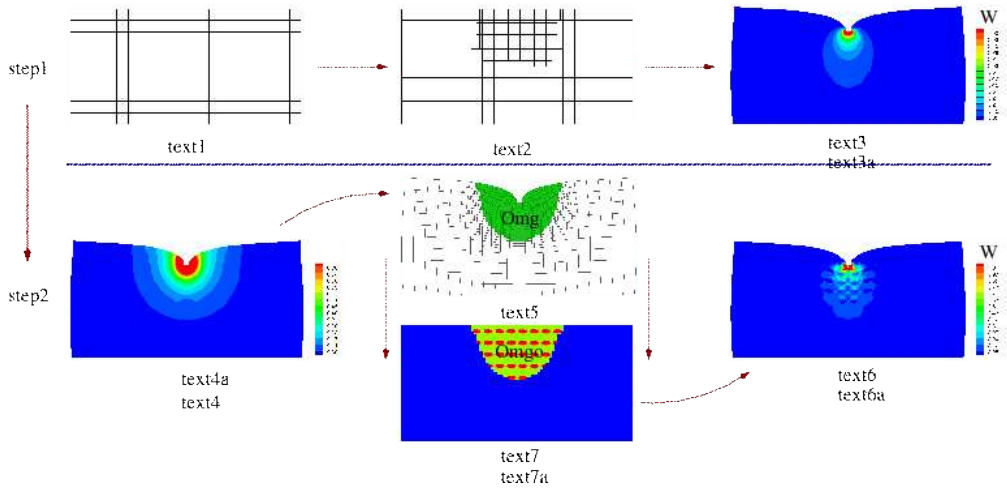

FIGURE 3. *The two stages of the scale adaptation algorithm are depicted: (*STAGE 1*) the homogenized solution is resolved, (*STAGE 2*) scale adaptation is applied within an indicated zone.*

[4] S. Ghosh, J. Bai, P. Raghavan, *Concurrent multi-level model for damage evolution in microstructurally debonding composites*, Mechanics of Materials **39** (2007), 241–266.

[5] L. Klinger, J. B. Vos, K. Appert, *A simplified gradient evaluation on non-orthonormal meshes: application to a plasma torch simulation method*, Computers & Fluids **33** (2004), 643–654.

[6] V. G. Kouznetsova, M. G. D. Geers, W. A. M. Brekelmans, *Multi-scale second-order computational homogenization of multi-phase materials: a nested finite element solution strategy*, Comput. Meth. Appl. Mech. Engrg. **193** (2004), 5525–5550.

[7] İ. Temizer, P. Wriggers, *An adaptive multiscale resolution strategy for the finite deformation analysis of microheterogeneous structures*, Comput. Meth. Appl. Mech. Engrg (2009–under peer review).

Research Report on Liquid Crystal and Membrane

PINGWEN ZHANG

A liquid crystal (LC) was first reported about 120 years ago by Reinitzer when he was studying the physical properties of cholesteryl esters. There are many different liquid crystalline subphases that have been identified and characterized. The nematic phase possesses the lowest order with only long range molecular orientational order as well as short range positional and bond orientational order. The next class of calamitic liquid crystalline phases is the smectic phase, which possesses layered structures. Depending upon the mesogen orientation within the layers, they can be smectic A (parallel to the layer normal) or smectic C (tilted from the layer normal). Liquid crystals can be divided into thermotropic and lyotropic LCs. Thermotropic LCs exhibit a phase transition into the LC phase as temperature is changed, whereas lyotropic LCs exhibit phase transitions as a

function of concentration of the mesogen in a solvent (typically water) as well as temperature.

The thermodynamic concepts of equilibrium and stability in phases and at phase transitions are important. The liquid crystal director is used as the order parameter to describe liquid crystalline phase transitions. Microscopic theoretical treatment of fluid phases can become quite involved, owing to the high material density, which means that strong interactions, hard-core repulsions, and many-body correlations cannot be ignored. In the case of liquid crystals, anisotropy in all of these interactions further complicates analysis. There are a number of fairly simple theories, however, that can at least predict the general behavior of the phase transitions in liquid crystal systems.

A very simple model which predicts lyotropic phase transitions is the hard-rod model proposed by Lars Onsager. This theory considers the volume excluded from the center-of-mass of one idealized cylinder as it approaches another. The fundamental insight here is that, while parallel arrangements of anisotropic objects leads to a decrease in orientational entropy, there is an increase in positional entropy. Thus in some case greater positional order will be entropically favorable. This theory thus predicts that a solution of rod-shaped objects will undergo a phase transition, at sufficient concentration, into a nematic phase.

The statistical theory, proposed by Dr. Alfred Saupe and Dr. Wilhelm Maier, includes contributions from an attractive intermolecular potential. The anisotropic attraction stabilizes parallel alignment of neighboring molecules, and the theory then considers a mean-field average of the interaction. Solved self-consistently, this theory predicts thermotropic phase transitions, consistent with experiment.

The existence of orientational order also means that a liquid crystal has cylindrical symmetry with the director as the axis of revolutionary symmetry. The stationary solutions with Maier-Saupe potential for liquid crystal were shown to be necessarily a set of axially symmetric functions, and a complete classification of parameters for phase transitions to these stationary solutions is obtained in [1,2].

From the perspective of dynamics, the motions of microscopic particles are vastly different in different phase structures. This difference introduces questions concerning how to quantitatively describe these motions and how the motions of each interacting particle contribute to the macroscopic phase properties. One needs to view the macroscopic thermodynamic properties of a system as an average of the microscopic mechanical motions of the particles. Statistical mechanics serves as a bridge to connect the macroscopic properties with microscopic motions.

The first systematic presentation of the statics of nematics is due to Frank. The Frank theory deals with orientational distortions, Frank demonstrated that an arbitrary distortion can be decomposed into three basic ones (splay, twist, bend). Ericksen and Leslie extended the continuum mechanical approach used by Frank in statics to encompass the dynamical behavior of nematics. The LE theory couples the director and the velocity fields via the appropriate choice of a constitutive equation for the stress tensor.

The molecular theory of liquid crystal is based on the rigid rod-like model. The great advantage of the rod-like model is that the molecular conformation is fixed once for all, and consequently, among the molecular coordinates, only position and orientation in space remain to be specified. The orientational distribution function plays a central role in the theory of rod-like molecules, the dynamical equations of the distribution function were introduced in a book by Doi and Edwards.

Liquid crystals are endowed with continuous symmetries and physical prevalence of correlations of positional orientation, thus show a rich and complex variety of topological defects. Defects in liquid crystals are of various dimensionalities, not only line defects, but also points, walls and configurations. Although many aspects of defects in liquid crystals are well understood, there is still a number of important problems to explore. The molecular theory of liquid crystal is useful to study the defects [3].

Lyotropic liquid-crystalline phases are abundant in living systems, the study of which is referred to as polymorphism. Accordingly, lyotropic liquid crystals attract particular attention in the field of biomimetic chemistry. In particular, biological membranes and cell membranes are a form of liquid crystal. Their constituent molecules are perpendicular to the membrane surface, yet the membrane is capable of a range of elastic stress, leading to some aspects of elastic behaviour to be exhibited. The constituent molecules can inter-mingle easily, but tend not to leave the membrane due to the high energy requirement of this process. Lipid molecules can flip from one side of the membrane to the other, this process being catalysed by flippases and floppases. These liquid crystal membrane phases can also host important proteins such as receptors freely "floating" inside, or partly outside.

The cell membrane is considered as a lipid bilayer where the lipid molecules can move freely in the membrane surface like fluid, while the proteins are embedded in the lipid bilayer. Beneath the lipid membrane, the membrane cytoskeleton, a network of proteins, linking with the proteins in the lipid membrane is neglected in the fluid mosaic model. Wolfgang Helfrich deduced the expression for the elastic energy of curvature per unit area of the membrane as

$$g_c = \frac{1}{2}\kappa(c_1 + c_2 - c_0)^2 + \tilde{\kappa}c_1c_2$$

where c_1, c_2 are two principal curvatures of the surface of the membrane, and the constant c_0 is called the spontaneous curvature of the membrane surface. The total bending energy of the membrane F is often referred to as the total bending energy of the membrane, is given by

$$F = \int g_c dA$$

The constant c_0 can be attributed to the mean curvature of the membrane with asymmetric chemical composition of layers in bilayer or the environment and is closely related to the 'spontaneous splay' of the liquid crystals. The constant κ is the bending rigidity and $\tilde{\kappa}$ is the elastic modulus of the Gaussian curvature. By comparing with the curvature elasticity of liquid crystals, both κ and $\tilde{\kappa}$ are found to be in the order of the product of the elastic constants of lipid bilayer and the

thickness of the membrane. The Helrich free energy of lipid membranes and is generally recognized as the basic quantity in dealing with the mechanical behavior of biomembranes in the liquid crystal phase.

The essential idea of Helfrich model is that the spontaneous curvature c_0 is strongly related to the orientational order parameters on both sides of the membrane. In mechanism, c_0 is strongly influenced by the changes in chemical structures of the molecules, the salinity and the temperature in the vesicle.

The extraordinarily beautiful and complex shapes of cells and cell organelles are fashioned by the physical forces that operate on their membranes. A fundamental problem of molecular cell biology in conjunction with physics and mathematics [4] is to understand the evolutionary, developmental and functional rationale for these shapes, as well as the mechanisms that are used by cells to produce them.

References

[1] Chong Luo, Hui Zhang and Pingwen Zhang, *The structure of equilibrium solutions of one-dimensional Doi equation*, **Nonlinearity**, 18, 379-389, (2005)

[2] Hailiang Liu, Hui Zhang and Pingwen Zhang, *Axial symmetry and classification of stationary solutions of Doi-Onsager equation on the sphere with Maier-Saupe potential*, **Communications in Mathematical Sciences**,3 201-218, (2005)

[3] Haijun Yu and Pingwen Zhang, *A kinetic-hydrodynamic simulation of microstructure of liquid crystal polymers in plane shear flow*, **Journal of Non-Newtonian Fluid Mechanics** 141 (2-3): 116-127 FEB 15 (2007)

[4] Dan Hu, Pingwen Zhang and Weinan E, *Continuum theory of a moving membrane*, **Physical Review E** 75 (4): Art. No. 041605 Part 1 APR (2007)

Reporter: Carsten Carstensen

Participants

Prof. Olivier Allix
L.M.T. Cachan
61 Avenue du President Wilson
F-94235 Cachan

Robert Altmann
Institut für Mathematik
Humboldt-Universität zu Berlin
Unter den Linden 6
10099 Berlin

Prof. Dr. Uri M. Ascher
Department of Computer Sciences
University of British Columbia
Vancouver , B.C. V6T 1Z2
CANADA

Dr. Daniel Balzani
Institut für Baumechanik und
Numerische Mechanik
Leibniz Universität Hannover
Appelstr. 9A
30167 Hannover

Dr. Sören Bartels
Institut für Numerische Simulation
Universität Bonn
Wegelerstr. 6
53115 Bonn

Prof. Dr. Leonid Berlyand
Department of Mathematics
Pennsylvania State University
University Park , PA 16802
USA

Dr. Alfonso Caiazzo
INRIA Rocquencourt
Domaine de Voluceau
B. P. 105
F-78153 Le Chesnay Cedex

Prof. Dr. Carsten Carstensen
Institut für Mathematik
Humboldt-Universität zu Berlin
Unter den Linden 6
10099 Berlin

Prof. Dr. Zhiming Chen
Institute of Computational Mathematics
Chinese Academy of Sciences
P.O.Box 2719
Beijing 100080
CHINA

Prof. Dr. Georg Dolzmann
Fakultät für Mathematik
Universität Regensburg
Universitätsstr. 31
93053 Regensburg

Dr. Aleksandar Donev
Computing and Mathematics Research
Division, Lawrence Livermore
National Laboratory
Livermore , CA 94330
USA

Dr. Maxim V. Fedorov
Max-Planck-Institut für Mathematik
in den Naturwissenschaften
Inselstr. 22 - 26
04103 Leipzig

Prof. Dr. Wolfgang Hackbusch
Max-Planck-Institut für Mathematik
in den Naturwissenschaften
Inselstr. 22 - 26
04103 Leipzig

Prof. Dr. Klaus Hackl
Lehrstuhl für Allgemeine Mechanik
Ruhr-Universität Bochum
Fakultät für Bauingenieurwesen
Universitätsstr. 150
44801 Bochum

Prof. Dr. Ralf Kornhuber
Institut für Mathematik
Freie Universität Berlin
Arnimallee 6
14195 Berlin

Dr. Frederic Legoll
LAMI-ENPC
6 et 8 Avenue Blaise Pascal
Cite Descartes - Champs sur Marne
F-77455 Marne la Vallee Cedex 2

Prof. Dr. Ping Lin
Dept. of Mathematics
University of Dundee
23 Perth Road
GB-Dundee DD1 4HN

Caroline Löbhard
Institut für Mathematik
Humboldt-Universität zu Berlin
Unter den Linden 6
10099 Berlin

Prof. Dr. Mitchell B. Luskin
School of Mathematics
University of Minnesota
127 Vincent Hall
206 Church Street S. E.
Minneapolis MN 55455-0436
USA

Prof. Dr. Axel Malqvist
Dept. of Information Technology
Uppsala University
Box 337
S-75105 Uppsala

Prof. Dr. Pingbing Ming
Institute of Computational Mathematics
Academy of Mathematics and Systems Sc.
Chinese Academy of Sciences
No. 55, Zhong-Guan-Cun East Road
100 190 Beijing
P.R. CHINA

Dr. Christoph Ortner
Mathematical Institute
Oxford University
24-29 St. Giles
GB-Oxford OX1 3LB

Prof. Dr. Eun-Jae Park
Computational Sciences & Engineering-WCU
Yonsei University
Seoul 120-749
KOREA

Dr. Daniel Peterseim
Institut für Mathematik
Humboldt-Universität zu Berlin
Unter den Linden 6
10099 Berlin

Prof. Dr. Petr Plechac
Department of Mathematics
University of Tennessee
121 Ayres Hall
Knoxville , TN 37996-1300
USA

Prof. Dr. Andreas Prohl
Mathematisches Institut
Universität Tübingen
Auf der Morgenstelle 10
72076 Tübingen

Dr. Serge Prudhomme
ICES
The University of Texas at Austin
1 University Station, C0200
Austin TX 78712-0027
USA

Prof. Dr. Weiqing Ren
New York University
Courant Institute of Mathematical Sciences
251 Mercer Street
New York , NY 10012
USA

Dr. Tomas Roubicek
Mathematical Institute
Charles University
Sokolovska 83
186 75 Praha 8
CZECH REPUBLIC

Dr. Giovanni Samaey
Departement Computerwetenschappen
Katholieke Universiteit Leuven
Celestijnenlaan 200A
B-3001 Heverlee

Prof. Dr. Jörg Schröder
Institut für Mechanik
Universität Duisburg-Essen
45117 Essen

Prof. Dr. Christoph Schwab
Seminar f. Angew. Mathematik
ETH Zentrum
HG G 58.1
Rämistr. 101
CH-8092 Zürich

Dr. Yi Sun
Courant Institute of
Mathematical Sciences
New York University
251, Mercer Street
New York , NY 10012-1110
USA

Prof. Dr. Anders Szepessy
NADA
The Royal Institute of Technology
Department of Mathematics
S-10044 Stockholm

Prof. Dr. Peter Wriggers
Institut für Kontinuumsmechanik
Leibniz Universität Hannover
Appelstr. 11
30167 Hannover

Prof. Dr. Harry Yserentant
Institut für Mathematik
Technische Universität Berlin
Straße des 17. Juni 136
10623 Berlin

Andreas Zeiser
Fachbereich Mathematik
Technische Universität Berlin
Straße des 17. Juni 136
10623 Berlin

Prof. Dr. Pingwen Zhang
School of Mathematical Sciences
Peking University
Beijing 100871
P.R. CHINA